POLITECNICO DI TORINO

Master of Science in Mechanical Engineering

Master's Degree Thesis

Finite Element Analysis by Using Cohesive Interface Element in Double Cantilever Beam

Supervisor:

Prof. Giovanni Belingardi

Candidate:

Sena Beyter

Co-supervisor:

Ph.D. Dario Fiumarella

October 2021

ABSTRACT

Delamination is a phenomenon of degradation of composite laminates that may lead structures to failure or that may reduce their stiffness and strength. Finite element analysis using the Cohesive Zone Method (CZM) is a widely used method for analyzing delamination in laminated composites.

The aim of this thesis is to examine the effect of DCB geometry and mesh size on the delamination length of the cohesive material and to present the numerical model closest to the our experimental result.

In order to eliminate the convergence problem of the mesh size, which is the main factor for the estimation of the process length, we prefer explicit analysis instead of implicit analysis. When modeling our DCB model with Explicit Time Integration (central difference diagram)and Time Step Significance amd Courant-Friendrichs-Lewy(CFL) characteristic length, we show that not only the mesh size is the most important factor in reaching the test results,also that the number of layers the result even if the same height is selected.

Keywords: Double Cantilever Beam, Delamination, Cohesive Zone Method, Finite Element Analysis, Explicit Time Integration.

ACKNOWLEDGEMENT

I would like to thank my esteemed advisor, Prof. Giovanni Belingardi, who undertook my consultancy in my master's thesis, encouraged me with his positive attitude and I am proud to be his student.

I would like to thank Ph.D. Dario Fiumarella, who showed great effort during the thesis period, did not spare me his support and patiently answered all my questions.

I would like to thank my boyfriend and colleague Ammar Salem, who believed in me during this challenging period of my life, and who I patiently overcame every challenge with him, and also inspired by him.

I would like to express my gratitude to my mother and sister who have stood by me all my life, supported me and made great sacrifices.

INDEX

LIST OF FIGURES

LIST OF TABLES

CHAPTER 1

INTRODUCTION

Today the search for a product that requires high performance despite its lightweight has required the intensive use of composite material and has brought new methods along with the developing technology. For instance, laminated composites, which are preferred because of their performance, are stacked to provide an overall characteristic performance and high strength. Since there is no reinforcement throughout the thickness between the laminates, a cracking phenomenon called delamination occurs, which causes the layers to separate.

In this section, composite material and delamination phenomenon are explained, and then the fracture mechanism and cohesive zone method are explained, and finally why we preferred cohesive zone method is mentioned.

1.1 Composite Materials

Composite material is formed by a combination of different laminates consisting of unidirectional fibers embedded in a matrix material. The layers are stacked in different directions as they are expected to exhibit high strength-to-weight ratio and high stiffness-to-weight ratio in each of the fiber directions.

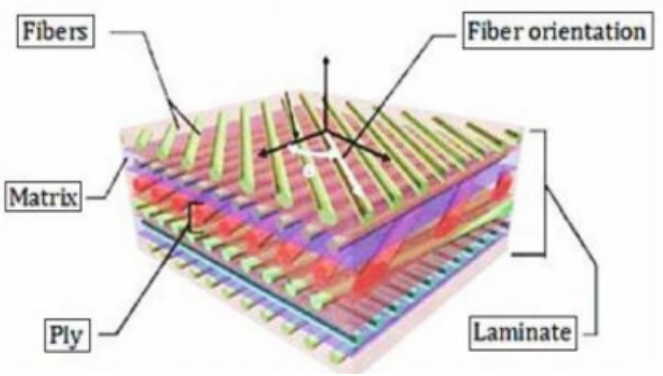

Figure 1.1 Illustration of composite laminated **[6]**

Although the need to develop lighter and stronger structures increases the use of composite materials with specific strength, durability, fatigue and corrosion resistance; since the onset of damage occurs inside the material, it makes it difficult to detect damage and the poor impact resistance limits the use of composite material **[40]**

1.2 Delamination Phenomenon

Delamination is a phenomenon of degradation of composite laminates that may lead structures to failure or that may reduce their stiffness and strength. Delamination in laminated composites develop three modes of interlaminar fracture.These are mode I, mode II and mode III.

The interlaminar tension (Mode I) is used in the fracture toughness test. Normal stress is in perpendicular to crack plane. In interlaminar shear (Mode II), crack surfaces slide over one in opposite directions but in same plane.In interlaminar scissoring (Mode III) crack faces are displaced parallel to the crack surface and parallel to the crack-tip. **[29]**

The interlaminar fracture toughness in the opening mode (Mode I) is determined using the double cantilever beam (DCB) specimen.

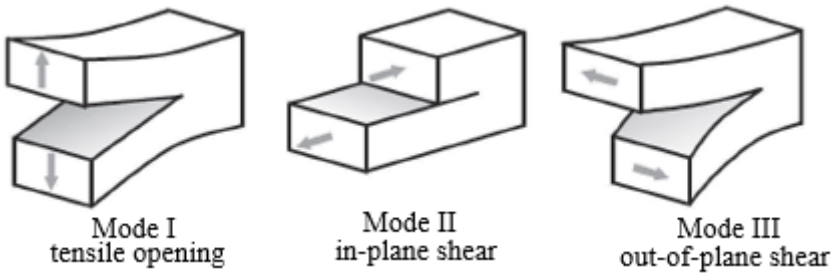

Figure 1.2 Failure mode in fracture toughness tests **[28]**

DCB specimen is made of unidirectional fiber reinforced laminate with even numbers of plies in 0° direction. A non-adhesive insert is placed at the mid plane near the loaded end in order to create an artificial crack.

Delamination phenomenon is divided into two parts as delamination initiation and delamination propagation.

1.2.1 Delamination Initiation

Delamination initiation analyses are usually based on the point or maximum stress criteria. Although strength of material criteria recognizes in plane failure modes, it is not sufficient out of plane cracks.Quadratic criterion is generally used in mixed-mode initiation problem.But this approach does not be used for specifying charecteristic length since no a material constant value has been proven.**[9]**

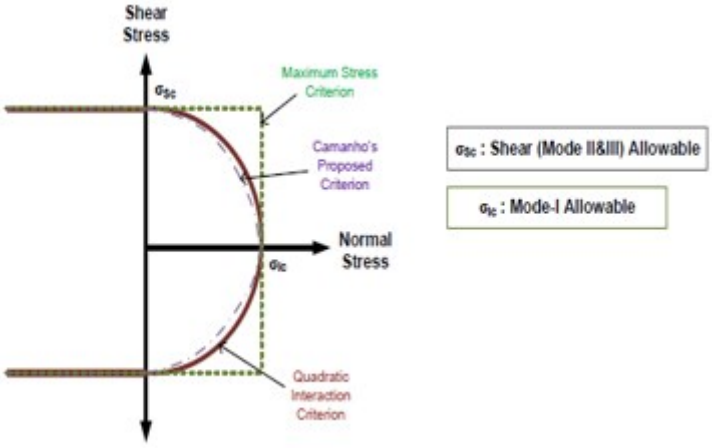

Figure 1.3 Delamination initiation criteria **[41]**

1.2.2 Delamination Propagation

Delamination propagation based on fracture mechanism and damage mechanism.

1.2.2.1 Fracture Mechanism

Linear elastic fracture mechanism, LEFM, assumes that a linear elastic body contains a sharp crack and then describes the energy change which occurs when such a body undergoes an increase in crack area. The most important point is that if there is no initial crack, LEFM procedure cannot be applied here.

According to linear elastic fracture mechanics, delamination growth is predicted when a combination of the components of the energy release rate is equal to, or greater than, a critical value. VCCT calculates energy release rate by using Irwin's crack closure integral, whereas, J-integral method, virtual crack extension and stiffness derivative use similar or modified procedures to predict delamination growth. **[5]**

Although LEFM-based data reduction procedures are used to determine fracture toughness of a composite with high confidence, Fracture toughness shows dependencies on loading rate and crack growth rate with changes in temperature and humidity conditions, but LEFM-based delamination growth analysis and data reduction procedure often neglect these effects.

VCCT is based on Irwin's crack closure integral. This method assumes that the energy needed to create the fractured surfaces is equal to the energy needed to close the fractured surfaces and crack growth occurs if the energy release rate reaches a critical value. Crack propagates just

along a predefined path. As the mechanical properties of laminate are better than matrix, crack branching is hindered and so the delamination propagation is bordered into resin rich interface.

This method, which has an advantage because it is a calculation based on energy rather than stress, is disadvantageous because it assumes linear elastic behaviour of the material before delamination onset. Crack initiation and the propagation of short cracks cannot be predicted. Only crack propagation could be predicted, regardless of crack initiation. It is not appropriated to analyse the damage tolerance of the structure. This technique needs nodal forces from nodes ahead and behind the crack tip for calculation.

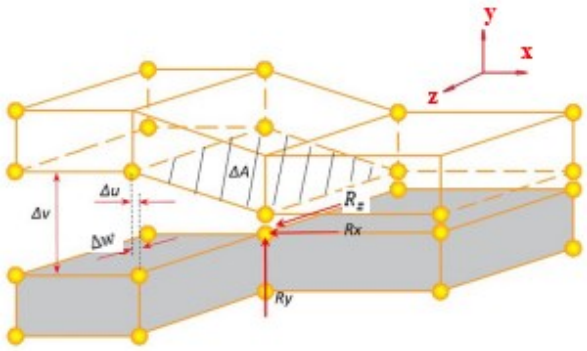

Figure 1.4 VCCT 3D Crack Model **[37]**

With the virtual crack closer technique, the strain energy release rate can be calculated successfully in both two-dimensional and three-dimensional laminar fracture analysis. However, there are some drawbacks that limit its use. Element size in a numerical model is an important factor for a successful result. The virtual crack closer technique, which has a finer mesh, requires long calculation times. Because finer element size along a crack path causes stresses at the free ends of the model to oscillate, numerical instabilities can occur and layers in the delaminated area may overlap. VCCT cannot predict the onset of delamination and requires knowing the presence of a pre-existing delamination. It is extremely difficult to predict the exact location of the delamination front using this technique, so its use alone is not sufficient for a comprehensive analysis of progressive delamination failure. For 2-D and 3-D crack geometry with a low order element mesh. Energy release rates are defined as **[37]:**

$$G_I = \frac{1}{2\Delta A} R_y \Delta v \qquad (1.1)$$

$$G_{II} = \frac{1}{2\Delta A} R_X \Delta u \qquad (1.2)$$

$$G_{III} = \frac{1}{2\Delta A} R_z \Delta w \qquad (1.3)$$

where R_x, R_y, R_z: reaction forces, $\Delta u, \Delta v, \Delta w$:relative displacement between top and bottom nodes of crack face, ΔE:work required to close the crack, ΔA:crack surface area, G_I, G_{II}, G_{III}:energy release rate. The model is assumed to be unit thickness, $\Delta A = \Delta a \times 1$ **[37]**

1.2.2.2 Cohesive Damage Mechanism

Cohesive Zone Modeling (CZM), also called Cohesive Damage Mechanism, combines the capability of continuum mechanics and fracture mechanics in describing the crack initiation and propagation stages. CZM describes ahead of the crack-tip using cohesive interface and traction separation law is used to eliminate the need to calculate the non-physical singular stress area at the crack tip.

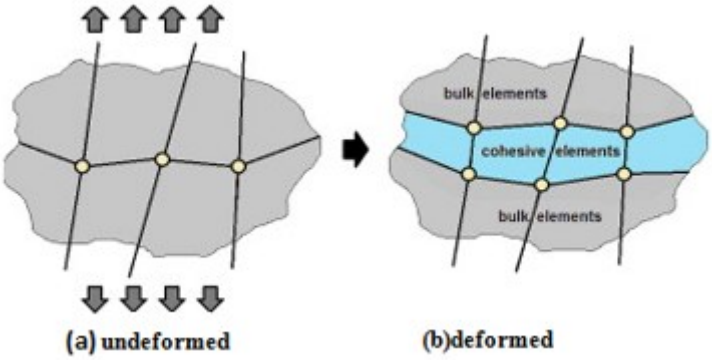

Figure 1.5 Mode I opening of cohesive zone element by traction **[3]**

Continuum model formulates the work conjugacy based on the stresses and strains, whereas tractions and displacement law is used to calculate the work conjugacy in the interfacial damage mechanics. Due to two different approach, interface problem was explained by thin adhesive layer assumption based on the continuum model by Allix and Ladev`eze (1992)**[4]**. According to this as the limit of the thickness tends to zero and induces a two dimensional behaviour,the stress distribution through the thickness of the layer is negligible and tractions at the upper and lower interfaces are accepted equal. This causes that tractions in the spring are uniform across the thickness.

Force-displacement relation is determined by CZM in shape of a traction-separation curve for each mode. This manages the behaviour of the element.Instead of strain,deformation is modelled by the relative displacement between the two surfaces interpolated to the Gauss points**.**

1.3 Comparison Between VCCT and Cohesive Zone Model

In our thesis, we aimed to observe the adhesive zone length and its relationship with the geometry of our model. Therefore, we used the cohesive zone model. Because instead of shaping the initial crack on the assumption of VCCT, we wanted to get more precise results with our CZM model with front crack length. In our study, we took into account that the mesh size effect can only be observed with CZM can be viewed in detail.

As a result of choosing the cohesive zone model, we were able to reveal both the onset of delamination and the propagation of delamination.Thus, we achieved more precise results.

COMPARISON BETWEEN VCCT AND COHESIVE ZONE MODEL

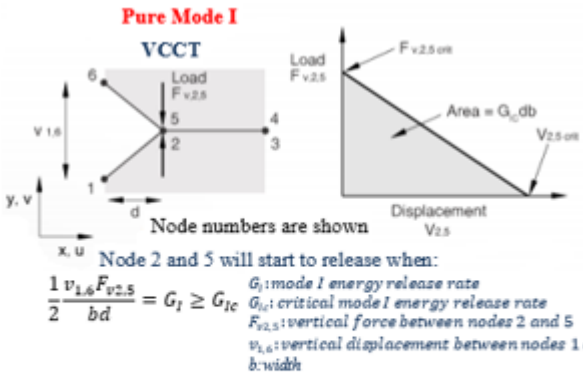

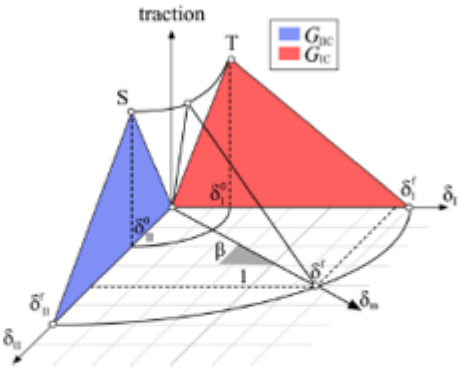

DIFFERENCES

VCCT	Cohesive Behaviour
Uses debond framework (surface based)	Interfaces elements (element based) or contact (surface based)
Assumes an existing flaw	Can model crack initiation. Damage initiation is based strictly on the predefined ultimate stress/strain limit.
Appropriate for brittle crack propagation problems.	Can be used for both brittle and ductile crack propagation problems
Brittle fracture using LEFM occurring along a well define crack front	Ductile fracture occurring over a smeared crack front modelled with spanning cohesive elements or cohesive contact
Requires G_I, G_{II}, G_{III}	Requires E,σ_{max}, G_I, G_{II}, G_{III}
Crack propagates when strain energy release rate exceeds fracture toughness.	Crack initiates when cohesive traction exceeds critical value and releases critical strain energy when fully open.
Crack surfaces are rigidly bonded when uncracked.	Crack surfaces are joined elastically when uncracked.
Available only in Abaqus/Standard	Available in Abaqus/Standard and Abaqus/Explicit.

Both theories: ➢ are used to model interfacial shearing and delamination crack propagation and failure. ➢ use an elastic damage constitutive theory to model the material's response once damage has initiated. ➢ dissipate the same amount of fracture energy between damage initiation and complete failure.

Table 1.1 Differences and similarities between VCCT and CZM

CHAPTER 2

COHESIVE ZONE MODEL

2.1 Background of Cohesive Zone Model

The first study of the cohesive zone model was done by Barenblatt in 1959, based on Griffith's theory of fracture, but there was no model yet to describe the true crack tip behavior. Dugdale(1960) stated that with the strip yield model, the stresses in the elastic-perfect plastic material are limited by the yield stress and a thin plastic region is formed in front of the crack tip. Barenblatt(1962) **[19]** introduced forces at molecular scale to this region, which Dugdale expressed, in order to eliminate the stress singularity at the crack tip and solve the equilibrium problem in elastic bodies, and defined the idea of the cohesive zone. However,contrary to their first approaches, the material does not show linear elastic behavior in the cohesive zone model and there is a finite stress value. Hillerborg (1976) **[23]** suggested that with the fictional crack approach, cohesive cracks will develop anywhere, even without the need for anterior crack, and that this is possible with tensile strength rather than molecular scale approach.

Hillerborg et al. (1976) made the first study on brittle fracture, while Needleman (1987) **[20]** did the first to model ductile fracture in the literature by explaining the polynomial traction-separation law. In Needleman's work in 1990, **[21]** he proposed a compressive normal force to prevent interpenetration of surfaces. But due to no constraints of this force were defined, the constant increase of interfacial penetration posed a problem at the surface.Then in his other study(1992),he introduced irreversible separation behaviour and according to him, cohesive strength depended on a damage variable.Tvergaard(1990) **[15]** with trapezoidal law, focused on this irreversible character of softening behaviour and ensured that the traction-separation paths of the loading and unloading operations do not overlap.But unlike Tvergaard, Camacho and Ortiz (1996) **[17]** assumed linear dumping behavior and defined an infinite initial slope in their model.Xu ve Needleman (1993).**[11]** predicted normal and shear traction.They explained reversible(elastic) behaviour by exponential traction law. Scheider et al.(2003) expressed a ductile tearing process with a traction and separation law for metallic materials.

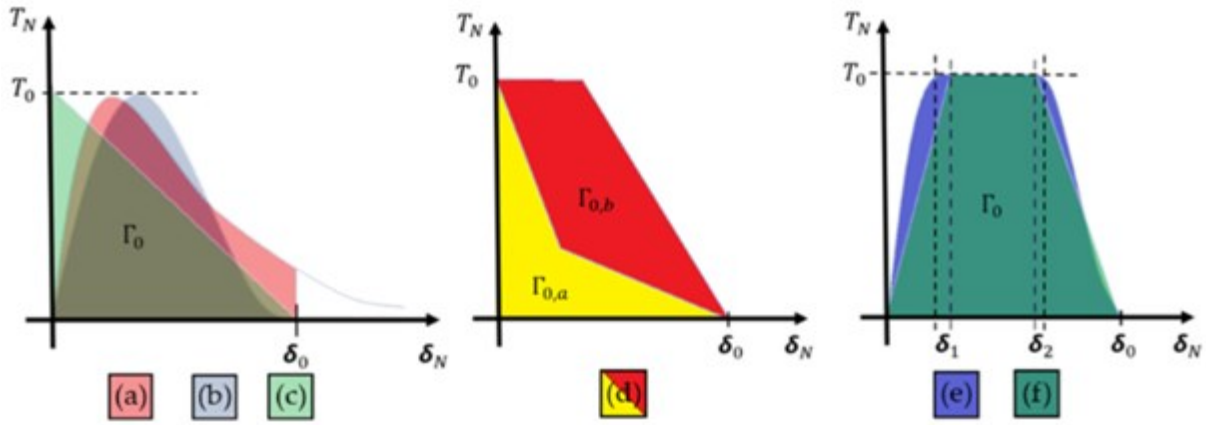

Figure 2.1 Types of traction separation laws a)Needleman 1987, b)Needleman 1990, c)Hillerborg 1976, d)Bazant 2002, e)Scheider and Brocks 2003, f)Tvergaard and Hutchinson 1992 **[14]**

Mi et al studied elastic snap-back instability in delamination propagation.Instability occurs after the stress has passed its peak. This problem occurs in that coarse mesh of interface also has high strength and high initial stiffness.They suggested using a fine mesh as a solution, which can be achieved with at least two cohesive elements in the cohesive zone in front of the crack tip. Mi et al. (1998) **[25]** defined the bilinear traction-separation model and Alfano(2001) **[30]** showed that this model gives more accurate results than other traction-separation laws. In addition to this, Mi et al. showed that the 2D plane strain formulation can give precise results, just like the three-dimensional one.Moreover, they also used the modified cylindrical arc length method in their work.However, this method does not reduce the oscillations occurred during delamination, it only avoids numerical problems caused by oscillations and long calculation times is necessary is needed.

Alfano and Crisfield (2001) focused on tangent stiffness and they applied co-rotational formula for large displacement and rotations that realized based on mode I displacement and critical energy release rate. However, unlike using pure mode like Alfano and Crisfield, Camanho and Dávila (2007) **[28]** expressed with Benzeggagh and Kenane's law and used mixed mode for energy release rate and loading .

Turon et al.(2007) **[29]** focused their efforts on mesh density rather than network size to solve the convergence problem. They examined the effect of penalty stiffness on mesh density. They stated that in order to achieve maximum traction, there should be more than two elements in

the cohesion zone.Numerical study on the length of the cohesive zone was done by Harper and Hallet(2008) **[26]** They studied relation between interfacial strength and mesh size and suggested that there should be a limitation on the amount of reduction in interface strength due to excessive softening.

We used the approach of Alfano and Crisfield to see the co-rotation of our DCB at the end of the model. In addition, we benefited from the study of Turon due to the concept of mesh size, and finally Harper and Hallet, considering the effect of the penalty stiffness of the cohesive material on the result.

2.2 Cohesive Zone Model &Bilinear Constitutive Law

The processes of the adhesive zone model are explained in the picture below. Here we can analyze both the onset of delamination and the propagation of delamination in detail.

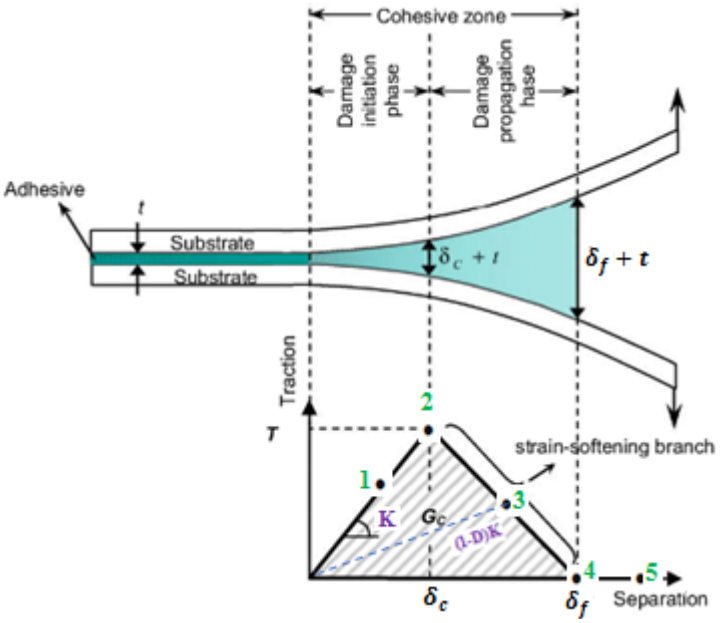

Figure 2.2 Bilinear constitutive law

In *elastic part*, as indicated by $\delta < \delta_c$,traction(τ)increases linearly as shown by point 1 until it reaches point 2, which indicates the maximum traction force. In this linear region expressed by stress-relative displacement equation $\sigma = K\delta$, there is no damage or discharge of the material. Slope of this part,K, gives elastic stiffness.

As expressed in interval $\delta_c < \delta < \delta_f$,from point 2, where the damage parameter "d" is equal to 0, to Point 4, where the parameter "d" is equal to 1, is called the "*softening part*".In this region,also called damage region, two layers separate from each other.Traction(τ) as shown

$\sigma = (1-d)K\delta$, across interface decreases until it is fully damaged.Area under the triangle (points 0,2,4) shows the fracture energy,which is the energy required to separate the two layers and it is also named 'energy release rate,G, in Ls-dyna.When loading has progress to the point 3 the material has suffered some damage but the layers have not separated yet. If unloading happens in this point, it is assumed to follow loading- reloading line from point 3 to point 0 and energy spent on partial damage to the bond is not recovered.

In decohesion part,as indicated by $\delta > \delta_f$, traction across interface the interface is null as shown in point 5.**[27]**

2.3 Cohesive Zone Length and Mesh Size

Defining the cohesive zone element mesh size requirements allows stable numerical simulations of interface delamination. If cohesive zone is discretized by too few elements (lower N_e,coarse mesh), delamination behaviour will not be captured as intended. Traction separation law requires very refined meshes ahead of the crack tip for stable crack growth.

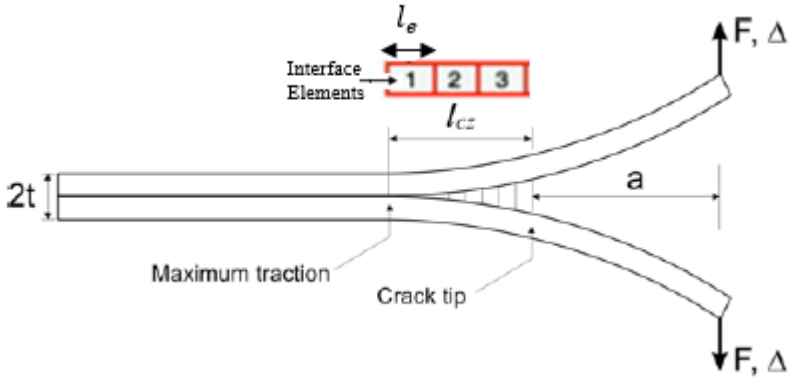

Figure 2.3 Cohesive zone length and mesh size in DCB **[2]**

In order to obtain the most consistent results in the literature, various studies have been made for the required number of elements at the interlaminar interface.Moes and Belytschko , based on the work of Carpinteri et al.,suggested using more than 10 elements.Falk et al**.[24]** used between 2 and 5 elements in their simulations.Mi et al. suggested to use at least 2 elements in the cohesive zone.Davila and Camanho,**[28]** who estimated the minimum element length as 1mm in their experiments and based on finding the cohesive zone length 3.28mm, stated that it would be sufficient to have 3 elements.Turon et al. (2007) and Harper and Hallett (2008)**[26]** suggested that for a fully developed cohesive region length, there should be at least three elements.

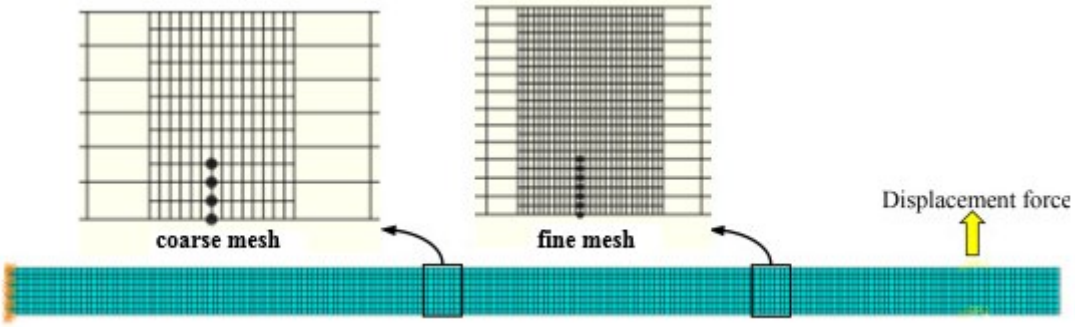

Figure 2.4 Coarse and fine mesh appearance in DCB **[36]**

Various studies have been made in the literature for the length of the cohesive region and different M values have been proposed.Turon included the following table in his research and stated that the M coefficient was consistent with his experiment at 0.88. Below are the reasons why other researchers use different coefficients, their studies and equations about the length of the cohesive region.**[29]**

Proposed by:	l_{cz}	M
Hui et al.	$\frac{2}{3\pi}E\frac{G_c}{(\tau^0)^2}$	0.21
Irwin	$\frac{1}{\pi}E\frac{G_c}{(\tau^0)^2}$	0.31
Dugdale,Barenblatt	$\frac{\pi}{8}E\frac{G_c}{(\tau^0)^2}$	0.4
Rice,Falk et al.	$\frac{9\pi}{32}E\frac{G_c}{(\tau^0)^2}$	**0.88**
Hillerborg et al.	$E\frac{G_c}{(\tau^0)^2}$	1.00

Table 2.1 Scale factor and cohesive zone length relation in DCB

Below, we explained in detail why other researchers use different coefficients and their work on the length of the cohesive region.

2.3.1 Irwin Approach

The Von Mises criterion in Irwin analysis was used to determine the size of the plastic region in the absence of an interface.Irwin focused only on extend of plastic zone along crack axis, not on its shape. According to Irwin, it was necessary to limit the stress values to the maximum limiting value, as stretching or more crack propagation would occur before the stress levels reached infinite values. **[5]**

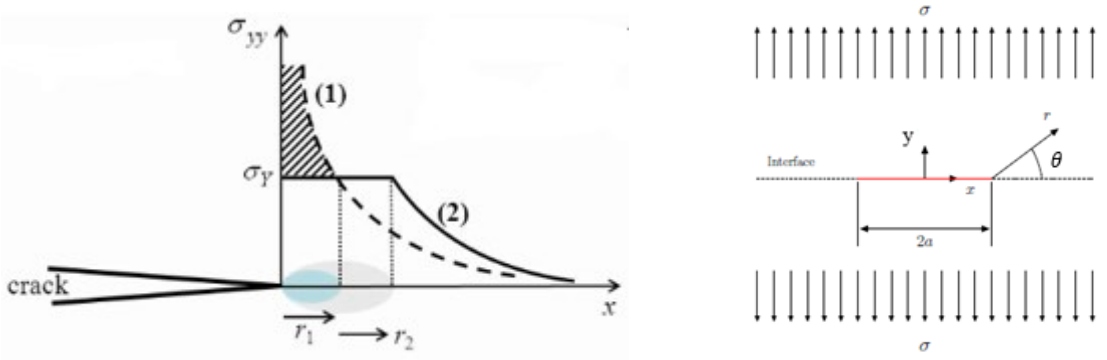

Figure 2.5 Irwin approach and stress value in plastic zone

$$\sigma_Y: uniaxial\ yield\ strength$$

$$\sigma_{xx} = \frac{K_I}{\sqrt{2\pi r}}\cos\left(\frac{\theta}{2}\right)\left[1 - \sin\left(\frac{\theta}{2}\right)\sin(\frac{3\theta}{2})\right] \quad (2.1)$$

$$\sigma_{yy} = \frac{K_I}{\sqrt{2\pi r}}\cos\left(\frac{\theta}{2}\right)\left[1 + \sin\left(\frac{\theta}{2}\right)\sin(\frac{3\theta}{2})\right] \quad (2.2)$$

$$(1) Elastic\ stress\ distribution:\ \sigma_{xx} = \sigma_{yy}(\theta = 0) = \frac{K_I}{\sqrt{2\pi r}} \quad (2.3)$$

$$(2) Elastic - Plastic\ stress\ distribution:\ \sigma_{yy} = \sigma_y\ ;\ r < r_2 \quad (2.4)$$

$$\frac{K_I}{\sqrt{2\pi r_1}} = \sigma_Y \Rightarrow r_1 = \frac{1}{2\pi}\left(\frac{K_I}{\sigma_Y}\right)^2 \quad (2.5)$$

Effective crack length: $a_{eff} = a + r_1$ (2.6)

Hatched area in figure cannot be carried in elastic-plastic material because stress cannot exceed yield .Plastic zone must increase in size in order to accommodate these forces. Irwin suggested correcting the stress distribution to restore balance. This is achieved by extending the process zone r_1 r_2 to , while the elastic zone shifts along the curve of the stress.

$$\sigma_Y r_2 = \int_0^{r_1} \left(\frac{K_I}{\sqrt{2\pi x}} - \sigma_Y \right) dx = 2 \frac{K_I}{\sqrt{2\pi}} r_1^{\frac{1}{2}} - \sigma_Y r_1 = \frac{{K_I}^2}{2\pi\sigma_Y} \tag{2.7}$$

$$r_2 = r_1 \tag{2.8}$$

Plastic zone length (plane stress):

$$2r_1 = \frac{1}{\pi}\left(\frac{K_I}{\sigma_Y}\right)^2 = M\left(\frac{K_I}{\sigma_Y}\right)^2 \tag{2.9}$$

Here $M = \frac{1}{\pi} = 0.31$ *and equal to scale factor in Irwin approach.*

2.3.2 Dugdale and Barenblatt / Yield Strip Model

Dugdale estimated the size of the yield zone ahead of a mode I crack in a thin plate of an elastic-perfectly plastic solid for limited plasticity(strip yield model) Barenblatt provided an analogue for ideally brittle materials of the Dugdale plastic zone analysis. According to their model is that stresses are finite in the strip yield zone, so there cannot be a singularity at the crack tip.

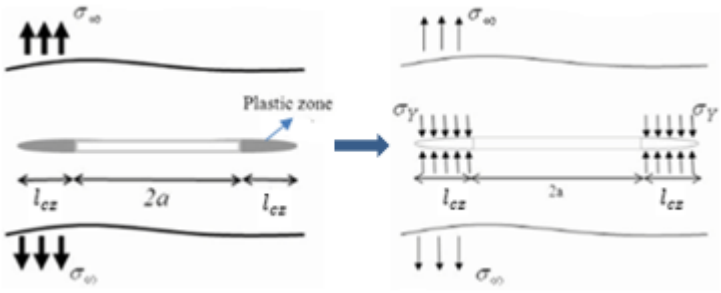

Figure 2.6 Front view of crack zone

This model is applied to a through thickness crack in an infinite plate and approaches the elastic-plastic behaviour superimposing remote tension and closure stresses at the crack:

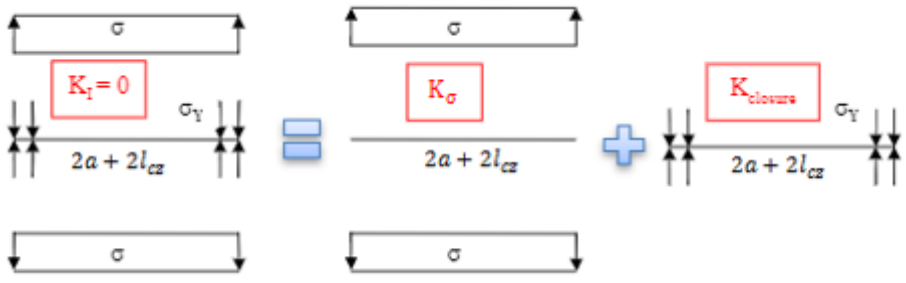

Figure 2.7 Superimposition remote tension and closure stress at crack **[35]**

They supposed that a crack length of 2a and plastic zones length l_{cz} ahead the real crack tips, works as if its length was $(2a + 2l_{cz})$ being the crack tips, l_{cz}, under a stress being equal to the yield stress. **[19]**

Stress intensity factor (SIF)from remote tension and closure stress cancel one other.

$$K_I = K_\sigma + K_{closure} = 0 \qquad (2.10)$$

After Stress intensity factor and Taylor series expansion operation, it can be obtained:

$$K_{closure} = -2\sigma_Y[(a + l_{cz})/\pi]^{1/2}.\cos^{-1}\left(\frac{a}{a + l_{cz}}\right) \qquad (2.11)$$

$$K_\sigma = \sigma.(\pi.(a + l_{cz}))^{1/2} \qquad (2.12)$$

We can obtain:

$$l_{cz} = \pi^2.\sigma^2.\frac{a}{8}.{\sigma_Y}^2 = \frac{\pi}{8}.\left(\frac{K_I}{\sigma_Y}\right)^2 = M.\left(\frac{K_I}{\sigma_Y}\right)^2 \qquad (2.13)$$

Here $M = \frac{\pi}{8} = 0.392$ is equivalent parameter or scale factor.

2.3.3 Hillerborg /Fictitious Crack Approach

Hillerborg(1976) assumed that the cohesive crack can develop anywhere, even if no preexisting macrocrack is actually present. According to this theory is that nonlinear behavior of the propagating crack is described by a fictitious crack with cohesive forces acting between its interfaces .At the crack tip maximum stress is equal to tensile strength and transmitted stress depends on the crack opening. This is defined by the strain softening diagram.The stress - separation function has an independent characteristic of structure, geometry, and size.If tensile strength,f_t, fracture energy, G_f,shape of stress separation curve ,f(w), are knewn,characterictic length can calculated.**[23]**

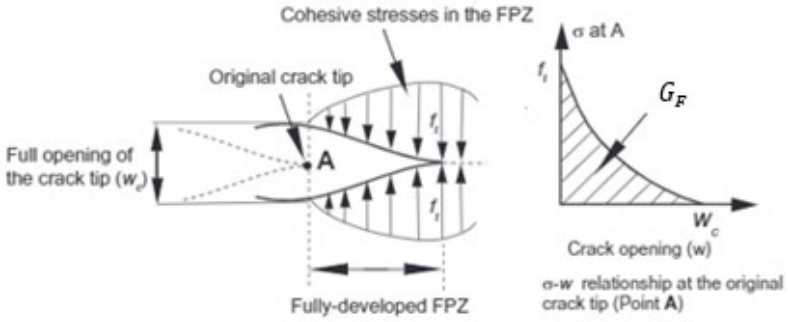

Figure 2.8 Fictitious crack approach

$$f(0) = f_t \tag{2.14}$$

$$\sigma = f(w) \tag{2.15}$$

$$G_F = \int_0^{w_c} f(w)dw \tag{2.16}$$

$$l_{cz} = \frac{E G_F}{{f_t}^2} \tag{2.17}$$

Where w_c: $critical\ crack\ opening$

Here M,scale factor, is equal to 1.

2.3.4 Rice et al./ Crack Front Waves and Cohesive Length

Rice and et al. studied the evidence of persistent crack front waves for a vectorial elasticity mode I crack.They stated that the Barenblatt-Dugdale type non-singular cohesive crack model,which is a non-perturbative numerical analysis of spontaneous fracture, coincides with the single crack-based approach ,when the R-dimensional region where the displacement attenuation occurs is much smaller than the other general length scales in the fracture problem.

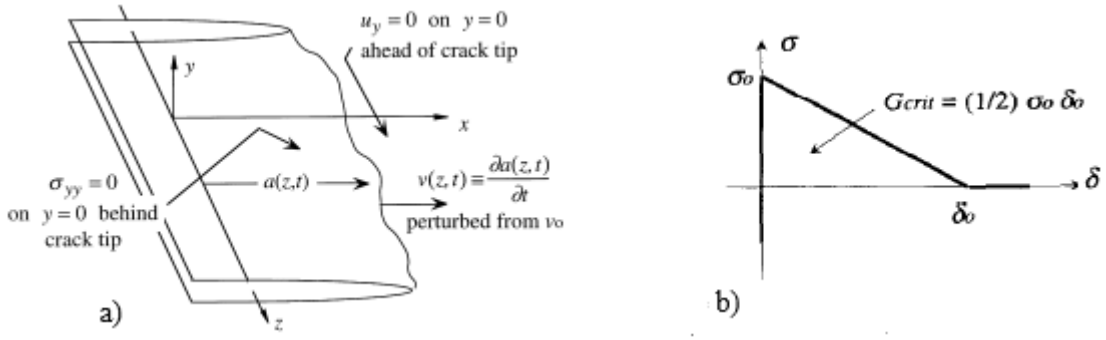

Figure 2.9 Singular crack model a)geometry of fracture b) traction-crack opening relation

Then Rice(1980) expressed these equations:

$$R = \frac{R_{v=0}}{f(v)} \text{ where } R_{v=0} \approx \frac{9\pi}{32}\left(\frac{M}{\sigma_0}\right)\delta_0 \qquad (2.18)$$

Where $R: length\ of\ region\ over\ where\ displacement - weakening\ occurs$,
$M: modulus\ of\ theory\ ;\ function\ f(v)\ where\ v: crack\ growth\ velocity$,
$\frac{\mu}{1-v}$: vectorial elasticity

Here $\frac{9\pi}{32} = 0.88$ is scale factor (M)for l_{cz}

2.3.5 Hui /Soft Elastic Solids

According to the theory, when the cohesive strength of the material is soft enough to exceed the elastic modulus of the material, the crack becomes blunt instead of spreading. The region in front of the blunt crack is called a cohesive zone. Crack opening is resisted by stretching the chains bridging the crack surfaces.

For high value of intrinsic fracture toughness of rubber : $G_c = G_c^o$ .Material is linearly elastic. So:

$$\sigma = \frac{K_I}{\sqrt{2\pi x}} \qquad (2.19)$$

Crack opening is resisted by the stretching of the chains bridging the crack faces.Cohesive zone length, L, is estimated by characteristic chain fracture stress equation.

$$\sigma_f = k_s \delta_{max} A \qquad (2.20)$$

$$L = \frac{{K_I}^2}{2\pi {\sigma_f}^2} \qquad (2.21)$$

For incompressible fluid energy release rate is related to stress intensity factor by $G = \frac{3K_I^2}{4E}$

$$L = \frac{2EG_c}{3\pi {\sigma_f}^2} \qquad (2.22)$$

$In\ this\ approach\ \frac{2}{3\pi} = 0.21\ is\ scale\ factor, M, of\ \ cohesive\ crack\ length(l_{cz})$

Where;

G_c: Energy release rate of rubber

G_c^o: Energy required to propagate

σ_f: $Fracture\ stress$

A: $area$

K_I: $Stress\ intensity\ factor$

E: $Young\ modulus\ of\ soft\ material$

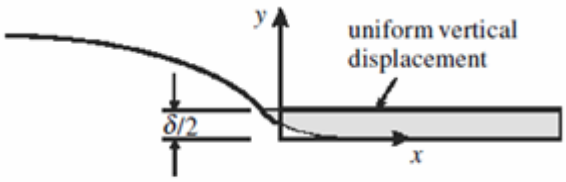

Figure 2.10 Opening displacement in DCB

2.4 Practical Solutions About Mesh size

The most important issue affecting the cohesive zone length is the mesh size. Although there is no consensus on the coefficient, there are many developments regarding the mesh size.It is known that a finer mesh will behave more realistically and lower peak interface traction force is needed for coarser meshes.When we focus on mesh size of the double cantilever beam (DCB) analysis.Figure 2.11 shows that 0.25 mm mesh is fully "converged" and further mesh refinement would not improve the accuracy. Also, the 0.5 mm mesh seems to be adequately converged.On the other side,4 mm mesh gives the peak load that is way too high.

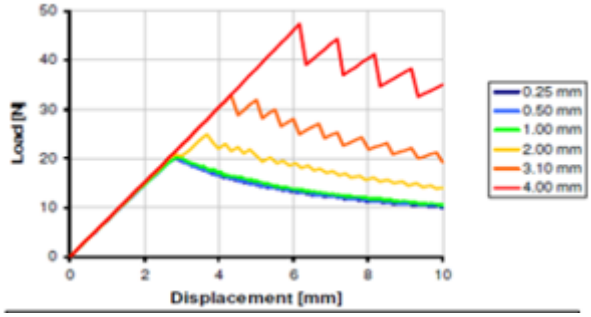

Figure 2.11 Load-opening displacement curve of different mesh sizes in DCB **[1]**

Energy release rates G_{Ic} and G_{IIc} are critically important for succesful analysis then interface (penalty) stiffness and peak tractions for tension and shear must be other priorities.They can be varied without affecting overall results much,as long as fracture toughness is correct.If the peak traction is lowered, the failure strain needs to be increased to keep the area under the curve correct.In this way, the effective element length increases and fewer elements are needed.

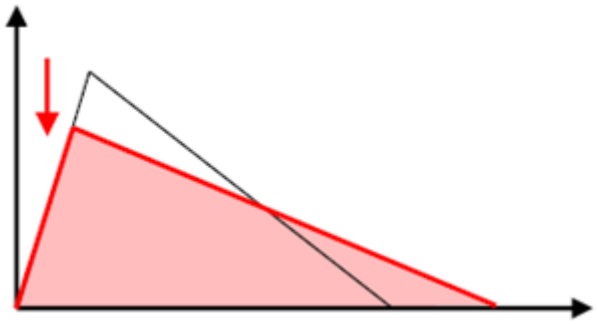

Figure 2.12 Lowering peak traction and effective element length

Bazant and Planas(1998) **[33]** also aimed to reduce the interface strength while keeping the fracture toughness constant, thus preventing the snap-back of the modified constituent model of large elements.They modified the constitutive model and define the characteristic element length. Thus they purposed that the calculated fracture energy is independent of discretization. According to Bazant's model, the strength should be adjusted by considering the size of the element perpendicular to the crack plane, when using crack band models in coarse mesh delamination simulation.

Alfano and Crisfield (2001) **[30]** used 0.25 mm element size, together with maximum interface strength, σ_{max}, equal to 57 MPa**.**After the experiments,they observed that although variations of the maximum interface strength will change the stress distribution in regions near the crack tip,lowering the interfacial strength can improve the convergence ratio of the solution.

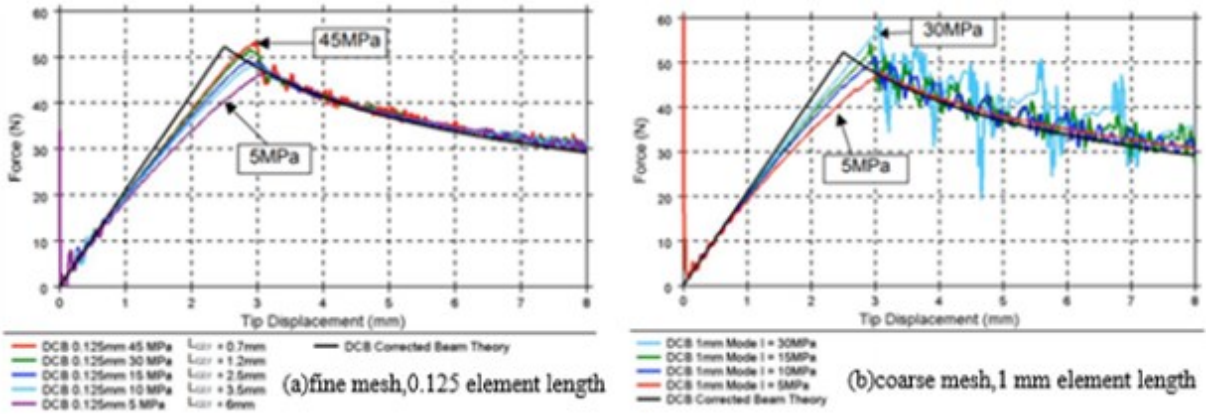

Figure 2.13 Effect of different interfacial strengths in mode I DCB model

Turon, Davila, Camanho, and Costa (2007) **[29]** stated that the 1 to 2 mm long cohesion zone requires at least three elements for accurate modeling and therefore the element size will be 0.3 to 0.6 mm in the direction in which the crack will propagate. After this non practical result,they have introduced a technique that allows larger elements and very fine meshes without compromising overall accuracy.Turon et al. (2007) and Alfano and Crisfield(2001)**[28]** aimed to reduce the interface strength to reduce the need for extremely fine meshes, thereby artificially increasing the length of the cohesive region, maintaining sufficient accuracy in calculating the energy release rate and being able to use larger elements. Alfano and Crisfield stated that artificially scaling the maximum traction stresses would alter the stress distribution within the structure, the solution would no longer reflect the correct mechanical behavior of the structure, so there should be a limitation in the length of the acceptable artificial cohesive region.

Relation between critical stress intensity factor K_c and critical energy release rate G_c can be expressed as $K_c^2 = G_c E$

Cohesive zone length, l_{cz} :

$$l_{cz} = ME_2 \frac{G_c}{{\sigma_{max}}^2} \tag{2.23}$$

$$l_e \leq \frac{l_{cz}}{N_e} \tag{2.24}$$

Where;

l_e: mesh size in direction of crack propagation; l_{cz}: length of cohesive zone;
M: scale factor; E_2: Transverse modulus of material;N_e: number of element

The analysis and test results of Turon for the cohesive region length were consistent with Rice's use of the scale factor , M = 0.88,defined, and therefore Turon was used as a coefficient of 0.88.

Above some approaches were explained relevant with mesh size and energy release rate effects for DCB. Due to convergence problem, we decided to use explicit method. In our thesis we preferred 0.75 for scale factor. First reason is Rice's and Turon's theory. Other reason is ls dyna gives interval between 0.65 to 1 in control card for this value. We used explicit analysis in DCB model and this value affects solution time. It was explained detail in chapter 5.

CHAPTER 3

DOUBLE CANTILEVER BEAM

3.1 Mode I Double Cantilever Beam Test

A double cantilever beam (DCB) test is used to determine of Mode I interlaminar fracture toughness,G_{Ic},of unidirectional fiber-reinforced polymer matrix composites by ASTM D5528 testing guideline **[34]**

DCB consists of two symmetrical adherent structures, one at the bottom and one at the top, with an adhesive embedded between them. In front of this adhesive located in the middle plane, there is a rectangular area where there is no adhesive to initiate delamination. It has uniform thickness, unidirectional laminated composite. Load is applied in opposite directions and perpendicular to the specimen by means of hinges or loading blocks from the free front end. When separating the lower and upper beams, the relationship between the load and the length of the delamination is calculated by looking at the front free ends.

There are some criteria and limitations in creating DCB specimen according to ASTM D5528 standards. Thickness of double cantilever beam must be between 3 and 5 mm. If loading blocks are used and accurate results are aimed, ratio between crack length and DCB thickness must be higher than 10 to apply data reduction process (a/2h >10).

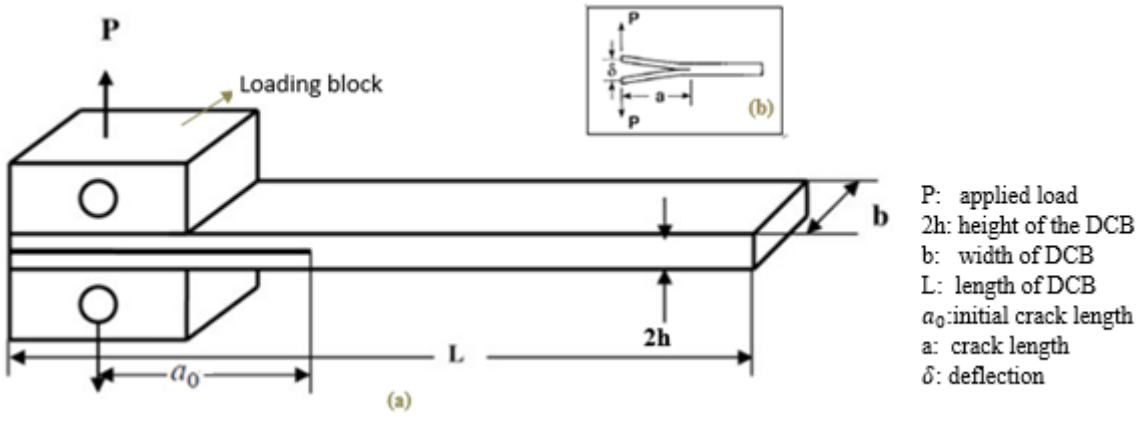

Figure 3.1 DCB test specimen (a)before test (b)after final displacement

Mode I interlaminar fracture toughness is calculated by a modified beam theory or compliance calibration method.Unlike given stiffer results by fixed clamped arm assumption, clamped elastic arm suppose that clamped surface is rotated during loading due to shear deformation of it.Considering this situation, using Willims' approach will give more accurate results.Because Williams, with modified beam approach, made a more efficient calculation by taking into account the effects of tip rotation at the crack tip, the effects of transverse shear, and the size-dependent effects of loading blocks.

According to elactic beam theory, deflection of beam's upper or lower arm is expressed:

$$\frac{\delta}{2} = \frac{P{a_0}^3}{3EI} \tag{3.1}$$

Modified beam theory is expressed by Williams who modified crack length:

$$\delta_i = \frac{2P(a_0 + \chi_l h)^3}{3E_{11}I} \tag{3.2}$$

Based on Williams 'Load' & 'Load and displacement' expression, χ_l:correction parameter can found.

$$\chi = \sqrt{\frac{E_{11}}{11G_{12}}}\left[3 - 2\left(\frac{\Gamma}{1+\Gamma}\right)^2\right]^{\frac{1}{2}} \tag{3.3}$$

Where:

$$\Gamma = 1.18\frac{\sqrt{E_{11}E_{22}}}{G_{12}} \tag{3.4}$$

Load P and δ has lineer relation in first region.After this point energy release rate G_I reaches critical energy release rate G_{Ic}.Thus propation of delamination starts ($G_I = G_{Ic}$) :

$$G_I = \frac{P^2(a + \chi_1 h)^2}{bE_{11}I} \tag{3.5}$$

At the end of delamination propagation,final deflection is expressed with:

$$\delta_f = \frac{2(bE_{11}IG_{Ic})^{\frac{3}{2}}}{3E_{11}IP^2} \tag{3.6}$$

Initial crack length a_0 instead of crack length a ,and G_{Ic} instead of G_I. Use G_I equation as showed above .Critical load at end of initial crack (delamination onset point):

$$P_c = \frac{\sqrt{G_{Ic}bE_{11}I}}{a_0 + \chi_1 h} \tag{3.7}$$

Fracture toughness and delamination length relation is expressed with R -curve.Initiation and propagation of delamination occur different critical fracture toughness from each other in 0/0 stacking unidirectional specimen. If $0°\frac{}{0}°$ stacked unidirectional specimen is used in DCB, fiber bridging creates resistance to the growth of the delamination. But this problem does not occur if each of upper and lower laminates have multiple layers of different orientation. Because of this reason, Solaimurugan and Velmurugan **[43]** investigated fracture toughness of multilayer laminates with different orientation angles.

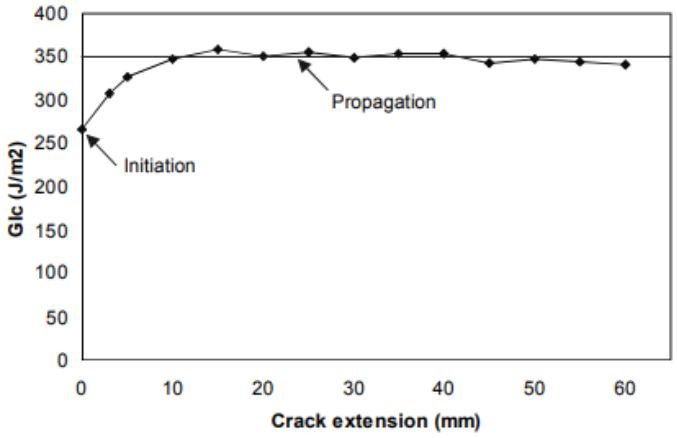

Figure 3.2 Fracture toughness of DCB during delamination

To solve the problem of crack jumping and uneven bending stiffness associated with the use of multi-directional laminate with different $\frac{\theta}{\theta}$interfaces, Robinson and Song **[43]** used a modified double cantilever beam (MDCB).They showed that the crack could propagate without fiber bridging and crack skipping at +45/+45 and +45/-45 interfaces. However, it was observed that the fracture toughness of the unidirectional 0º fiber composite was smaller. Therefore, DCB specimen must be preferred unidirectional 0º/90 º and include an even number of plies.

3.2 Effect of DCB Geometry in Cohesive Zone Length

This solution is based on elastic bending theory and linear elastic fracture mechanics. Material is assumed elastically isotropic and homogenous. We will use Castigliano's second theorem in following equations to substitute. So, we need to explain it firstly. **[42]**

Castigliano's second theorem: The first partial derivative of the total internal energy in a structure with respect to the force applied at any point is equal to the deflection at the point of application of that force in the direction of its line of action. The second theorem of Castigliano is applicable to linearly elastic structures with constant temperature and unyielding supports.

U_{pot}: potential energy of DCB:

$$U_{pot} = U_{strain} - P\delta \tag{3.8}$$

Where U_{strain}:strain energy of DCB, P:load of DCB in vertical direction, δ:crack tip opening displacement.

Strain energy of beam due to bending:

$$U_{strain} = \int_0^l \frac{M^2}{2E'I} dx \tag{3.9}$$

With l:length of DCB, M:applied moment, E':elastic modulus, I:second moment of inertia of beam. We identified 2 different I due to upper and lower beams and I_3 of DCB occurred.

$$U_{strain} = \int_0^a \frac{(Px)^2}{2E'I_1} dx + \int_0^a \frac{(Px)^2}{2E'I_2} dx \tag{3.10}$$

$$I_1 = I_2 = \frac{bh^3}{12} = I\ ;\ \ I_3 = \frac{b(2h)^3}{12} = 8I \tag{3.11}$$

$$U_{strain} = \frac{P^2a^3}{3E'I} \tag{3.12}$$

Substituting (Eq 3.12) into (Eq 3.8) and using Castigliano's second theorem, tip opening displacement is found:

$$\delta = \frac{\partial U_{strain}}{\partial P} = \frac{2Pa^3}{3E'I} \tag{3.13}$$

Force displacement relation:

$$P = \frac{3E'I}{2a^3}\delta \tag{3.14}$$

Energy release rate during crack growth:

$$G_I = -\frac{1}{b}\frac{\partial U_{pot}}{\partial a} = \frac{P^2a^2}{E'Ib} \tag{3.15}$$

Crack remains same ,$a = a_0$,during $G_I < G_{Ic}$ condition.

$$P = \frac{3E'I}{2a_0^3}\delta \tag{3.16}$$

When critical energy release rate $G_{Ic} = G_I$, crack starts to propagate.Crack is obtained by using (Eq 3.15) for crack length a:

$$P = \sqrt{\frac{2}{3\delta}}(bG_{Ic})^{\frac{3}{4}}(E'I)^{\frac{1}{4}} \tag{3.17}$$

After delamination is completed for crack length a ,response :

$$P = \frac{3E'I}{2l^3}\delta \tag{3.18}$$

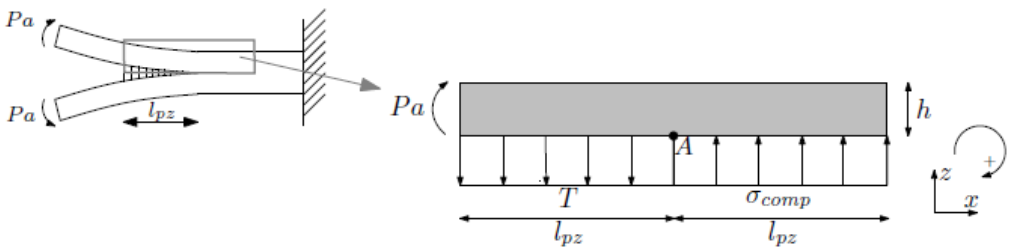

Figure 3.3 Cohesive zone region and compressive stress after delamination

Cohesive and compressive stresses are used even they are not equal:

$$Pa - \int_0^{l_{cz}} \sigma_{comp}(x)b\,dx - \int_0^{l_{cz}} T(x)b\,dx = Pa - bl_{cz}^2T_{max} = 0 \tag{3.19}$$

Substituting (Eq 3.19) into (Eq 3.15):

$$G_I = \frac{12 l_{cz}^4 T_{max}^2}{E' h^3} \tag{3.20}$$

Cohesive element length :

$$l_{cz} = h \left[\frac{G_{Ic}}{12 T_{max} h} \frac{E'}{T_{max}} \right]^{\frac{1}{4}} \tag{3.21}$$

To introduce dimentionless parameters D_1 and D_2, rewriting of equation:

$$l_{cz} = \left(\frac{1}{12} \right)^{\frac{1}{4}} D^{\frac{1}{4}} \tag{3.22}$$

$with\ D = D_1 D_2;$

$$D_1 = \frac{G_{Ic}}{T_{max} h} \quad \text{(3.23 a)} \qquad D_2 = \frac{E'}{T_{max}} \quad \text{(3.23 b)}$$

D_1:describes influence of interface properties on the cohesive zone length and D_2:describes ratio of bulk material stiffness and gives indication of deformation of bulk material as a result of interface traction.

DCB prediction does not affect cohesive zone length if $\frac{l_{cz}}{h} \ll 1$ (or $D \ll 1$). For values of D below 0.5, infinite geometry prediction.

DCB model was done in 6.9 mm height and it consists of 10 laminates totaly. When we look at the this theorem, we can tell that ratio between cohesive zone length and thickness of double cantilever beam is bigger than 1. So this situation will affect delamination of cohesive element. Considering the above formulas, we can say that cohesive zone length is affected positively bu using lower traction.Thus penalty stiffness must be chosen lower to contribute correct final delamination displacement in mixed mode rule.These factors will be explained in chapter 5 detail.

CHAPTER 4

DOUBLE CANTILEVER BEAM EXPERIMENT

4.1 DCB Experimental Methodology

Specimen were tested uniaxial testing machine according to ASTM D5528. In our experiment, samples were tested to determine static and fatigue delamination and based on cohesive zone model.

Each of the laminated beams is 150 mm long, 20 mm wide, 0.69 mm thick and consists of 10 layers. A thin film was used in preparation for the test. One side of this film was glued to the upper laminated beam and the other side to the lower laminated beam. The control of the beams was provided by hydraulic grips. Crack formation was initiated by pulling the two beams in the opposite direction. While the load displacement data was recorded, the sample reached the critical load, so the crack began to propagate. Small decrease in load was observed due to the increased compliance. The deflection was held constant, the separation of the beams stopped.

Since we aimed to achieve the correct energy release rate and delamination results during the DCB test and applied the mode-I traction-separation law, we used the Digital Image Correlation (DIC) technique in the experiment. So at the start of test, digital cameras were positioned in two places: one of them is at the crack tip and other is in the uncracked area. Because we aimed to observe a more clear displacement point. During the test, digital cameras measured the post-fracture length and photographs were taken. The experiment is carried out in loading stage accurately to determine the energy release rate.

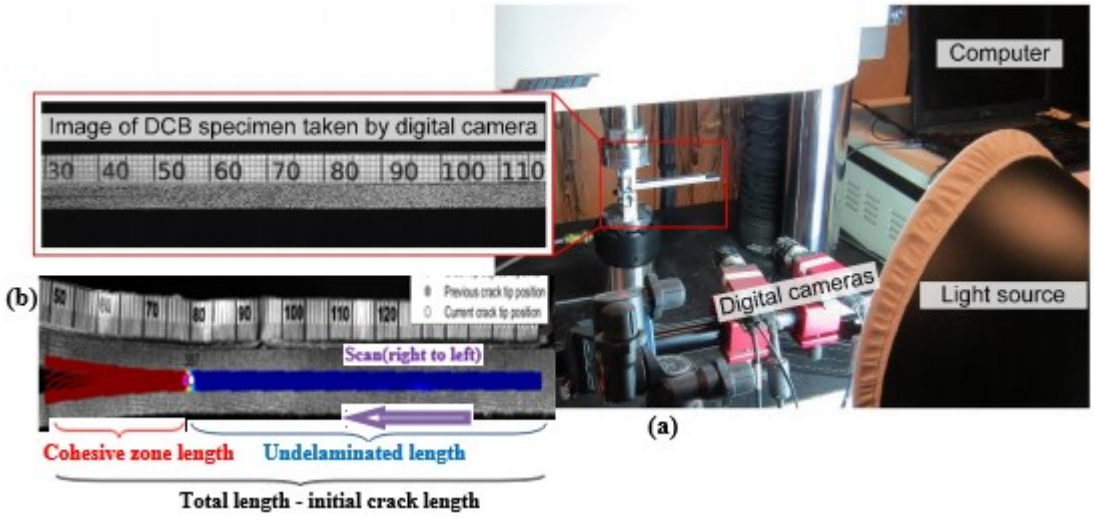

Figure 4.1 a)DCB test set up with DIC system b)determination of crack tip position from image of deformed DCB specimen

The laminates used in this test were pure polypropylene. Their stacking sequence is $\left[\frac{0_3}{0_3}\right]$. Its properties are specified in the table.

Dimensions and properties	
material	Pure polypropylene
shape	rectangular
length	150 mm
width	20 mm
Thickness of each laminate (h/2)	3.45 mm
pre-crack length	48.32 mm and 45.5 mm

Table 4.1 Dimensions and properties of DCB

4.2 Experimental Results

The cohesive law is formatted as a relationship between the traction σ and the displacement δ caused by the opening of the interface. The relationship between the traction that causes the interface to open and the displacement δ is formed according to this law. The picture below shows the photo of our specimen when it reached its maximum crack length.

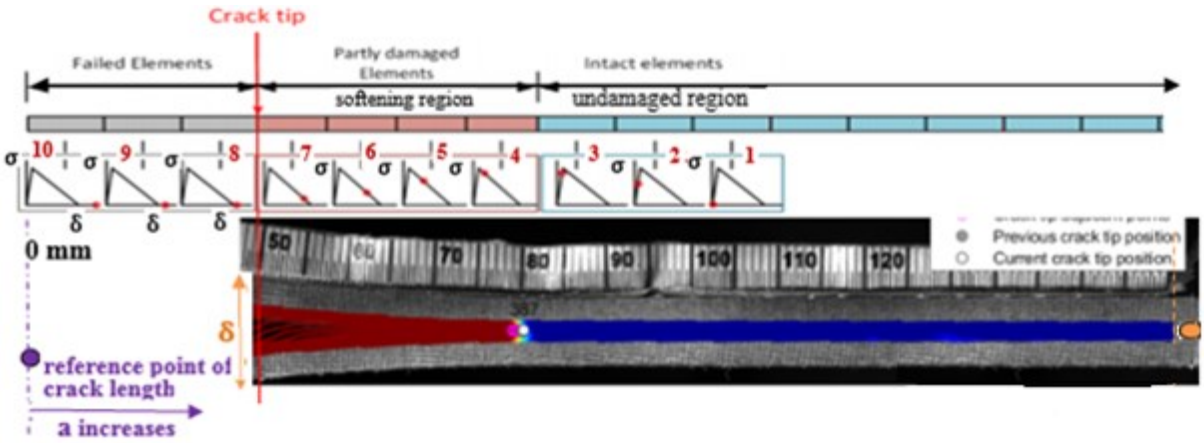

Figure 4.2 Digital image from experiment in frame 387

The fixed side of the sample, the point where the adhesive ends, is considered to be the starting point of the displacement in the literature. From this point until it reaches the initial displacement,δ_0,there is no damage to the cohesive element and the traction increases continuously. In our test result, we found the first value of opening displacement of 19.45 mm, which gave us the maximum traction (stress). We name the section up to this point as the undamaged area.When δ_0,is reached,damage accumulates in the element and therefore traction decreases until the final displacement, δ_f,is reached. As seen in the phased $\sigma - \delta$ curve,stress-opening displacement, in the picture, we reached δ_0 between the numbers 3 and 4, so we passed

to the softening zone, and at the end of the 7th curve we reached δ_f. In our test, we found this value, δ_f, 54.33 mm. So we arrived at the crack starting point. So the initial displacement,δ_0, gives us the maximum crack length,$a_0 + l_{cz}$, while the final displacement point , δ_f,gives us the initial crack length (a_0). The amount of change in crack length across the softening zone is called the cohesive zone length (l_{cz}).The remaining part after the 8. curve shows the first crack length zone, where there is no adhesive.

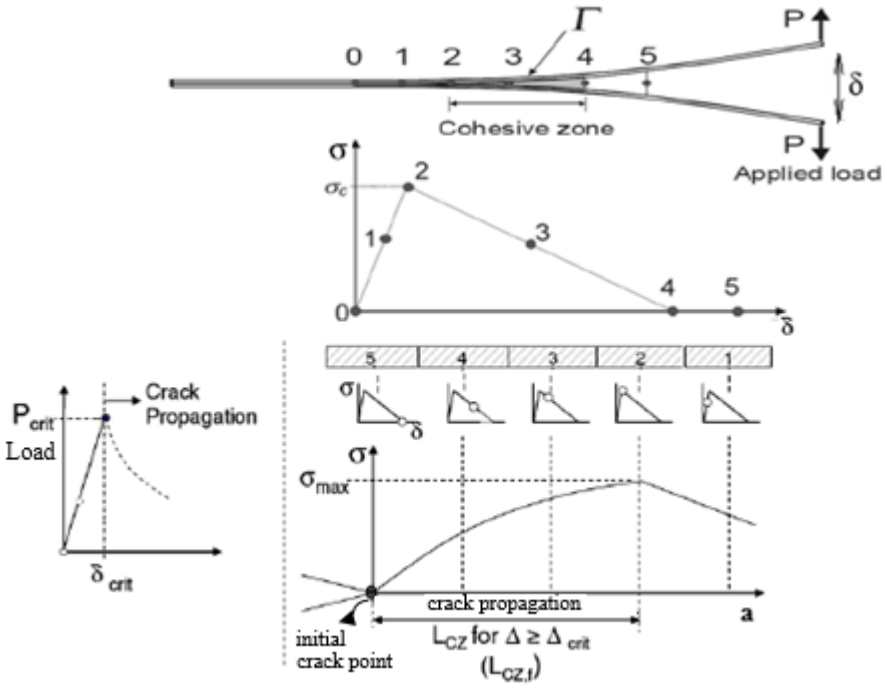

Figure 4.3 Crack propagation in Double Cantilever Beam

When the process is completed in the traction-displacement curve shown with 5 stages in the picture above, we actually have reached the zero point in the traction-crack curve. This point shows us the initial point. When we reach maximum traction, the change in crack length gives us crack propagation. In other words, this change is the part to the left of the maximum point in the crack curve, and the part to the right of the maximum point in the displacement curve.

As a result of the DCB test we have done, the data of two of the test samples are available in the table below. After the test results, we understand that it is better to take the specimen 1 as a reference. Because when we looked at the data, we saw that the second sample did much more oscillation after the softening zone. But according to literature, after reaching to crack tip, when the crack starts propagating, energy release rate value becomes constant. Moreover, this value does not depend on initial crack length.

DCB Mode I Experiment Results	Specimen 1	Specimen 2
Initial crack length a_0	48.32 mm	45.5 mm
Final crack length	148.661 mm	131.561 mm
Cohesive zone length l_{cz}	81.0592 mm	65.52 mm
Initial opening displacement δ_0	10.3214 mm	12.35 mm
Final opening displacement δ_f	54.34 mm	53.70 mm
Max Load P	29 N	29.15 N
Max Energy Release Rate GI	0.48 N/mm	0.36 N/mm

Table 4.2 : Experiment results of two DCB specimens

As seen in the test result graph of specimen 2, fibre bridging continues until a=66.03 mm from 45.5 initial crack length, it reaches max energy release rate value and anymore must not oscillate a lot from this limit.While load is decreasing time by time after at 66.03 mm ,GI shows increases more. This can be due to the size of the sample or rough surface effect.

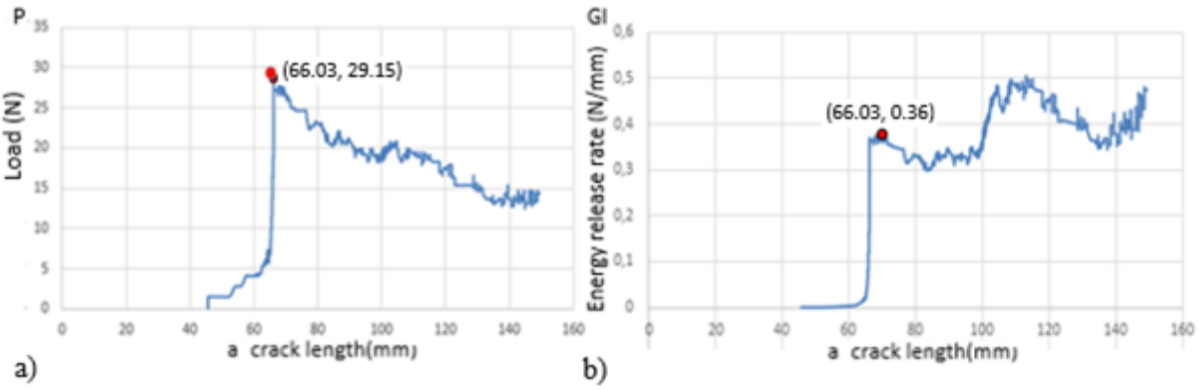

Figure 4.4 Test results of specimen 2 a) P-a curve, b) GI-a curve

In the test result graph of specimen 1,unlike the specimen 2, its load and energy release rate graphs gave more consistent results as expected. In the graphs of our test result below, the results of load-displacement and load-crack length are examined. According to crack curve; maximum delamination continued up to 148.61 mm crack length.Thus cohesive zone length was found 81.05 mm. When displacement curve is looked, it starts with intake element and shows elastic deformation then it reached starting of delamination point at 10.32 mm (δ_0). After right side of this point ,damage evaluation starts.When the end of the sample was reached, the test was ended and the displacement of 54.33 (δ_f). mm was recorded.

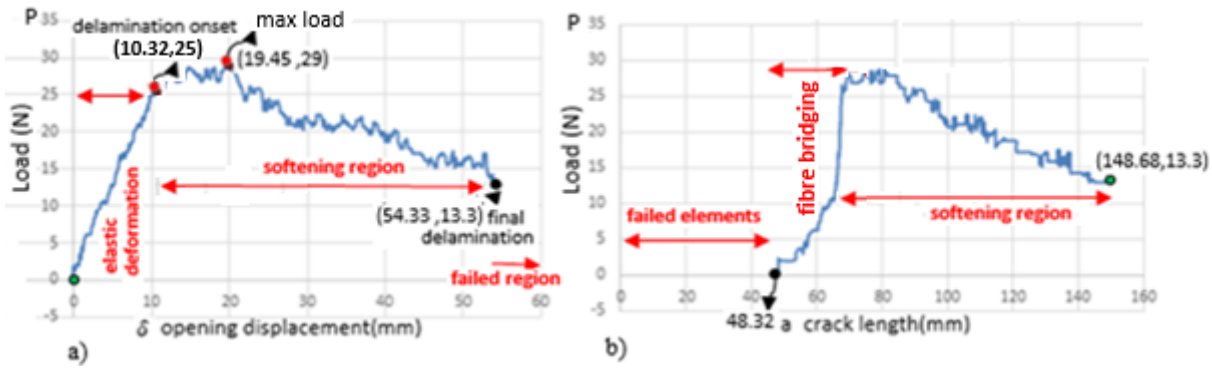

Figure 4.5 a) Load-displacement curve b) Load-crack length curve of speciment 1

When we look at the energy release rate-crack length curve called resistance curve (R curve), we see that fiber bridging takes place between 67.93 mm and 65.43 mm crack, the resistance to delamination growth increases and therefore delamination is slowed down. Previous studies have shown that increasing the stress intensity factor will be a solution to this problem. When we look at the crack point of 148.66 mm, we can see that the length of the cohesive zone reaches 81.05 mm despite the resistance. When this point is reached, the damage calculation is completed.

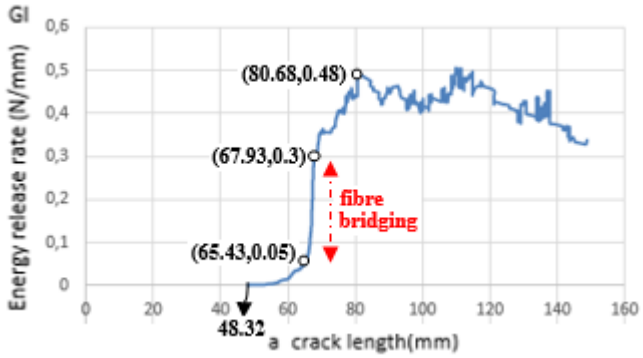

Figure 4.6 Energy release rate-crack length curve of experiment result

Point at crack tip position, $a_0 = 48.32\ mm$, load changed between 0-2 N and it contributed balanced at a=53.14 mm.

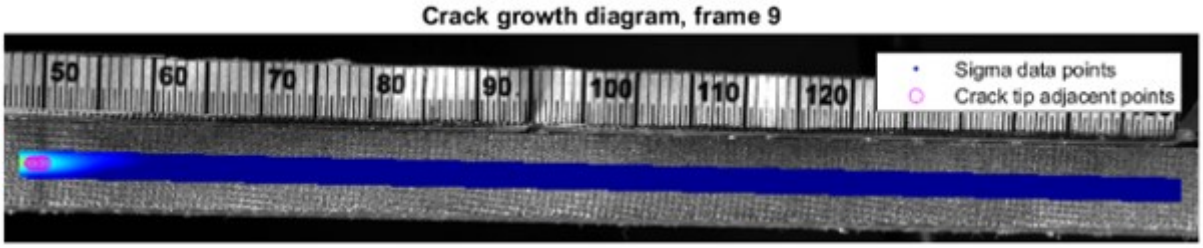

Figure 4.7 Digital image experiment result at frame 9

The picture below shows the state of the beam at $\delta_0 = 10.32\ mm$ critical delamination point. This point is also called the delamination onset.

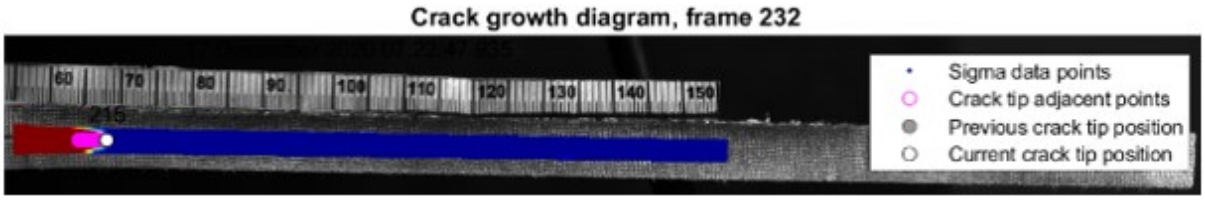

Figure 4.8 DCB at delamination onset point

The picture below shows the end of delamination, when the cohesive zone reaches 81.05 mm and the crack length is 148.66 mm.

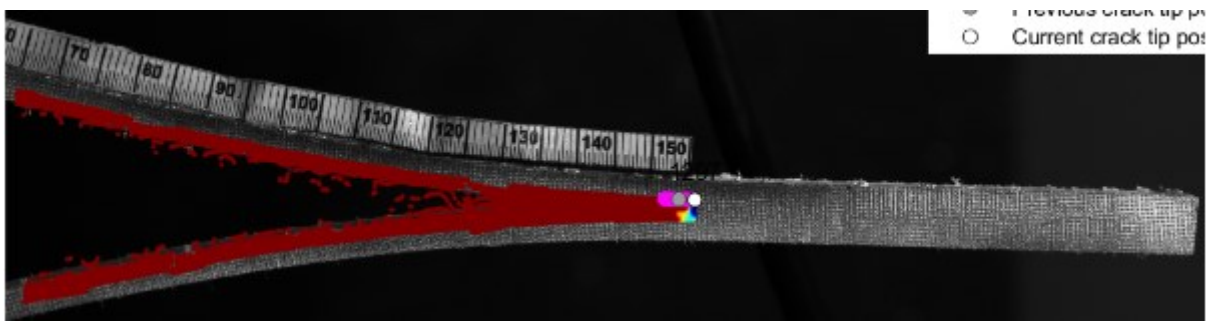

Figure 4.9 DCB at final delamination point

It is of great importance that our model, whose test results are as above, is analyzed with the finite element method and the results are compared. The point we need to focus on here is that the adhesive area between the beams is actual provided by a hot press. In the next section, our aim is to demonstrate that the material card we use for the adhesive area gives the same numerical values as our test result using the most appropriate values.

CHAPTER 5

FINITE ELEMENT MODELING OF DOUBLE CANTILEVER BEAM

5.1 Finite Element Formulation of Cohesive Zone Model

The use of a cohesive model allows to predict the onset and growth of delamination with more effective results. Almost zero thickness cohesive element is used to model the interface between laminates.Because it is embedded between laminates without affecting whole part. For this reason, cohesive zone models depend on displacements instead of strains (Davila et al.,2001).

Mat 138 cohesive mixed mode is based on bilinear traction-separation law with quadratic mixed mode delamination criterion and a damage formulation.It describes purely elastic cohesive zone and no plasticity is available here.It determines number of integration points required to delete the item with INTFAIL.

Based on the Chang -Chang failure criterion, the MAT 54 Enhanced Composite Damage card is used to describe the material properties of multilayer laminates. The use of 8 node cohesive element allows to overcome numerical instabilities.Laminates must be shell or Tshell Type 20 in the use of this card figure 5.1(b). Because critical time step of Type 19 managed by characteristic stiffness and mass of element rather than chacteristic length.

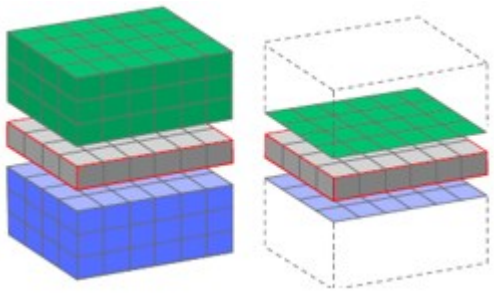

Figure 5.1 a) 8 node type 19 Elements b) 8 node type 20 **[39]**

Tiebreak condition does not sustain enough loading until crack propagation is initiated. Unlike the cohesive model, it requires tuning and gives unstable curve. For this reason, when we wanted to choose between solid or shell form based on cohesive modeling, we preferred Tshell element that gives the closest result to the analytical solution. Because in solid elements, traction-separation curve is not as smooth as analytical solution even it gives good responce.

Expression in theory	Material card-138 (cohesive)	Description	Units
σ_{max}	T	Peak traction in normal direction	MPa
τ_{max}	S	Peak traction in tangential direction	MPa
α	XMU	Exponent for mixed mode criterion	Unitless
G_I	GIC	Energy release rate for Mode I	N/mm
G_{II}	GIIC	Energy release rate for Mode II	N/m
δ_I^f	UND	Ultimate displacement in normal direction	mm
δ_{II}^f	UTD	Ultimate displacement in tangential direction	mm
K_n	EN	Normal stiffness (penalty stiffness)	N/mm^3
K_t	ET	Tangential stiffness	N/mm^3

Table 5.1 MAT 138 Cohesive mixed mode bilinear law parameters

They have more pronounced boundary conditions than shell elements, but they show lower performance than shell elements in thin-walled structures due to shear lock behavior. Thick-shell element includes an additional strain component across the thickness. Fully integrated 2D shell elements gives more accurate results in the initiation and propagation of delamination.

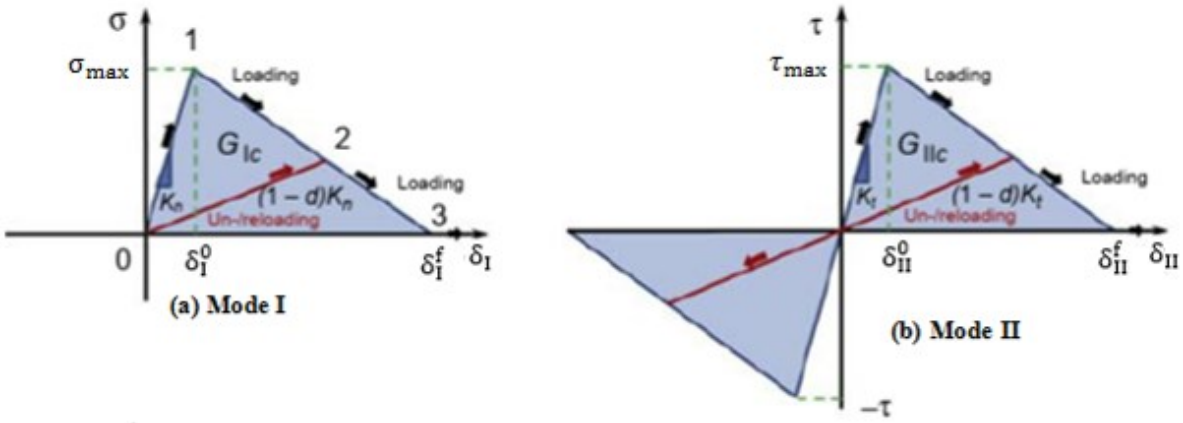

Figure 5.2 Bilinear traction separation law a) mode I b) mode II

Mode I (pure mode) :

Initial displacement in normal direction: $$\delta_I^0 = \frac{T}{EN} \quad (5.1)$$

Delamination propagation starts when single mode displacement reaches: $$\delta = \delta_I^0 \quad (5.2)$$

Ultimate displacement in normal direction: $\delta_{\mathrm{I}}^{\mathrm{f}} = UND = \frac{2G_{Ic}}{T}$ (5.3)

Failure occurs, when single mode displacement reaches: $\delta = \delta_{\mathrm{I}}^{\mathrm{f}}$ (5.4)

Mode II:

Initial displacement in tangential direction $\delta_{\mathrm{II}}^{0} = \frac{\mathrm{S}}{\mathrm{ET}}$ (5.5)

Ultimate displacement in tangential direction: $\delta_{\mathrm{II}}^{\mathrm{f}} = \mathrm{UTD} = \frac{2\mathrm{G_{IIc}}}{\mathrm{S}}$ (5.6)

Loading and unloading behaviour can occur during propagation process and in this sitution it reaches initial point of bilinear law.In this situation So power law is applied for predicting delamination propagation under mixed mode loading. Because it gives linear relation between energy release rates.XMU coefficient is positive when it is applied for pure mode in DCB specimen. Different approach is Benzeggagh-Kenane law that suggested by Camanho et al. But this method not used for Mode I and XMU coefficient is negative in BK law.

$\beta = \frac{\delta_{\mathrm{II}}}{\delta_{\mathrm{I}}}$ is defined mode mixity where: $\delta_{\mathrm{II}} = \sqrt{{\delta_1}^2 + {\delta_2}^2}$ (5.7)

Based on Power law,ultimate mixed-mode displacement δ^f is :

$$\delta^f = \frac{2(1+\beta^2)}{\delta^0}\left[\left(\frac{EN}{GIC}\right)^{XMU} + \left(\frac{ET \times \beta^2}{GIIC}\right)^{XMU}\right]^{\frac{1}{XMU}} \quad (5.8)$$

To assure that maximum load is before the failure point, formula is checked:

$$\frac{\delta_I^f}{\delta_I^0} = \frac{2G_I}{K_n LL} = \frac{2G_I}{K_n\left(\frac{T}{K_n}\right)^2} > 1 \quad \text{for tension} \quad (5.9)$$

$$\frac{\delta_{II}^f}{\delta_{II}^0} = \frac{2G_{II}}{K_t LL} = \frac{2G_I}{K_t\left(\frac{S}{K_t}\right)^2} > 1 \quad \text{for pure shear} \quad (5.10)$$

Cohesive zone length is calculated according to study of Turon et.al (2007):

$$l_{cz} = ME_{11}\frac{G_{Ic}}{(\sigma_{max})^2} \tag{5.11}$$

where cohesive zone length l_{cz}, element size l_e, longitudinal young modulus of material, E_{11} (EA value from card Mat 58 laminated composite fabric),scaling factor M is given 0.88. like it explained in the other chapter.

Number of element in fracture process zone, N_e, is calculated:

$$N_e = \frac{l_{cz}}{l_e} \tag{5.12}$$

Cohesive zone must have at least 3 number of element (Turon et.al 2007) **[29]**
For materials with low flexural modulus or high interlaminar fracture toughness, it may be necessary to increase the number of plies, that is increase laminate thickness or decrease delamination length in order to avoid large deflections of specimen arms.

DCB test specimen must contain even number of plies and must be unidirectional, with delamination growth occur in the zero degree direction.

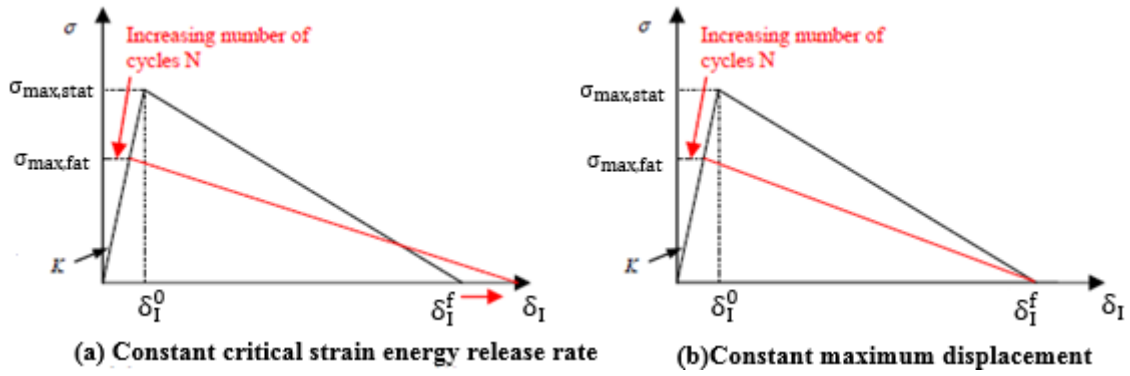

Figure 5.3 Modified traction displacement curve of DCB **[13]**

Based on Bazant and Planas(1998) **[33]** approch, we should aim to reduce the interface strength while keeping the fracture toughness constant, thus we can prevent snap-back of the modified constituent model of large elements. If the peak traction is lowered, the failure strain needs to be increased to keep the area under the curve correct.In this way, the effective element length increases and fewer elements are needed. So we prefer figure 5.3 (a) option.

5.2 Explicit Analysis of DCB

In this section, we aim to make our sample, which we modeled with Ls-dyna, which is one of the finite element method, consistent with the experimental results and then to increase the length of the cohesive region and to demonstrate the effect of the sample geometry on it.

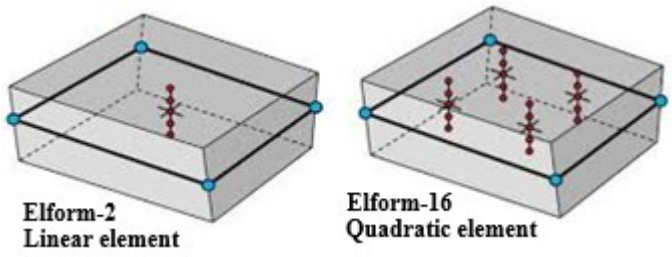

Figure 5.4 Difference between ELFORM 2 and 16 of shell DCB in Ls dyna **[18]**

In our model, instead of conventional elements, quadrilateral continuous shell element is selected. This is because the connection of cohesive elements to continuous shell elements is facilitated since there are common nodes at the interface. There are no cohesive elements at the interface with a 50 mm initial crack length and free nodes on either side of the sample is available.

When we examine the delamination length of the solid cohesive placed between the shell beams, it is seen that the mass plays an active role. In this case, dynamic analysis (explicit or implicit) is preferred instead of static analysis in modeling. We used explicit analysis based on stable time increment in our model, which gives us an advantage over implicit analysis as node accelerations are directly resolved and do not need to be iterated. Thus, we can avoid from convergence.

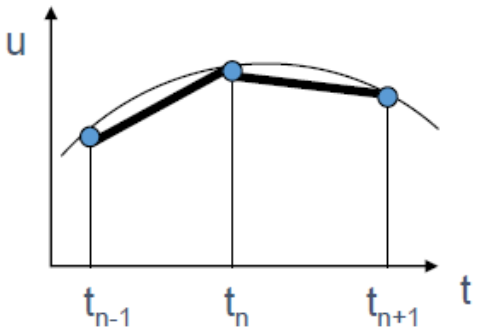

Figure 5.5 Central difference method in Explicit Time Integration

Here the maximum time step size is limited by the Courant condition. Velocity, mass and element size are important factors. According to this method, the velocity of a system whose acceleration is known in time n is calculated at n+1/2 and its displacement is calculated in time

n+1. A solution is developed by integrating acceleration into time. Strain is calculated by displacement, and stress is calculated from strain. **[12]**

$$\bar{\mathrm{M}} = \bigcup_{\mathrm{e}} \bar{\mathrm{M}}^{\mathrm{e}}, \qquad \bar{\mathrm{M}}^{\mathrm{e}} = \mathrm{M}^{\mathrm{e}} + \lambda^{\mathrm{e}} \tag{5.13}$$

$$\mathrm{U}^{\mathrm{t}+\Delta\mathrm{t}} = \mathrm{U}^{\mathrm{t}} + \Delta\mathrm{t}\dot{\mathrm{U}} + \frac{1}{2}\Delta\mathrm{t}^2\ddot{\mathrm{U}}^{\mathrm{t}} \tag{5.14}$$

$$\bar{\mathrm{M}}\ddot{\mathrm{U}}^{\mathrm{t}+\Delta\mathrm{t}} = \mathrm{R}^{\mathrm{t}+\Delta\mathrm{t}} \tag{5.15}$$

$$\dot{\mathrm{U}}^{\mathrm{t}+\Delta\mathrm{t}} = \dot{\mathrm{U}}^{\mathrm{t}} + \frac{1}{2}\Delta\mathrm{t}\left(\ddot{\mathrm{U}}^{\mathrm{t}} + \ddot{\mathrm{U}}^{\mathrm{t}+\Delta\mathrm{t}}\right) \tag{5.16}$$

$$\Delta\mathrm{t} = \alpha\Delta\mathrm{t}_{\mathrm{crit}} \tag{5.17}$$

where $\bar{M}$: *mass matrix*; $U, \dot{U}, \ddot{U}$: *nodal displacement, velocity, acceleration*; R: *nodal residual force*

λ^e: added artifical mass , Δt: *CFL timestep* , α: *scale factor*, Δt_{crit}: *explicit timestep*

Stable time increment is proportional to the shortest element dimension.Efficiency is increased by scaling mass density of critical element.But we must remember that using of cohesive element reduces time increment due to its small thickness.Explicit time increment for shell element :

$$\Delta Texplicit_{timestep} = \Delta t_{stable} \leq \frac{l_e}{c_m} = \frac{l_e}{\sqrt{\frac{E}{\rho(1-v^2)}}} \tag{5.18}$$

$$c_m = \sqrt{\frac{E_m}{\rho_m}} \tag{5.19}$$

$$\Delta Ttimestep_{CFL} = 0.75 \times \Delta Texplicit_{timestep} \tag{5.20}$$

Where c_m: $wave\ speed$, E_m: $young\ modulus$, ρ_m: $density$, l_e: $mesh\ size$, 0.75: $scale\ factor$

Explicit time integration (central difference scheme) consists of two parts. First one is Time Step Significance and it is based on Courant-Friedrichs-Lewy (CFL) characteristic length. According to this: velocity wave of material never exceed velocity of sound. Effective plastic strain is inversely proportional with element area (${l_e}^2$). Coarse or fine mesh is important criteria to contribute stable propagation as in equation of $\Delta t_{stable} \leq \frac{l_e}{c_m}$

Second method is Explicit Time Step Mass Scaling. It is based on *Control Timestep card and *Control Termination card. We used this method in our study. Explicit integration in our model: is shaped by DT2MS, TSSFAC and ENDMASS. Time step size, DT2MS, must be chosen less than zero, Ls Dyna adds mass of element whose timestep is below $|DT2MS|$ thus element's DT is equal to $|DT2MS|$. Scale factor, TSSFAC, can be between 0.65-0.9 and it affects time CPU. If it is bigger value of it will decrease simulation time.

$$\Delta\text{Timestep}_{\text{CFL}} = \text{TSSFAC}\frac{\text{min length}_{\text{element}}}{\sqrt{\frac{\text{E}}{\rho * \text{Mass scaling}}}} \qquad (5.21)$$

In our DCB is preferred 0.75 value and $TSSFAC \times |DT2MS| = const$ is minimum time step size permitted and mass scaling is done and if it is used to meet the Courant time step size criterion for transient analyses. Added mass can be observed with *DATABASE card of GLSTAT for all model.

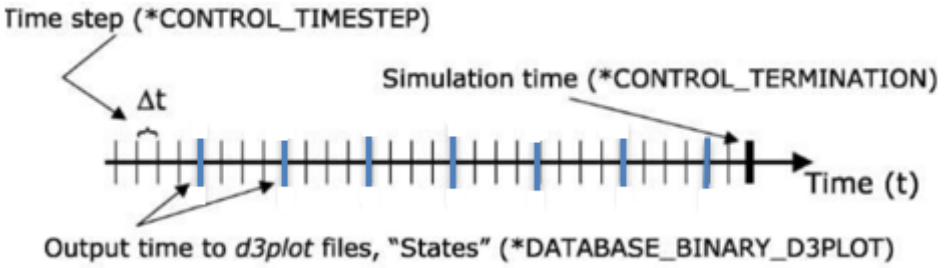

Figure 5.6 Solution time and output in explicit time integration **[16]**

Quadrilateral shell elements was used in the model. They have four nodes with six degrees-of-freedom at each node: x, y, z displacements and rotations.The nodal displacements are determined from the displacements at the Gauss points using the Midlin theory of plates and shells. Increasing the number of integration points through-thickness increases the accuracy and however it causes increasing of computational cost too.

Double cantilever beam consists of one shell element with using of *Part Composite card instead of *Element Shell Composite card in our study for the model delamination. One integration point is available for each layer. Elform 20 is used in zero thickness solid cohesive element to contribute coherence with Elform 16 shell integrated quadrilateral beam. Single-point integration is preferred instead of 8 Gaussian points in cohesive elements. Because it requires less effort calculate to strain matrix for each element than 8 Gaussian points.

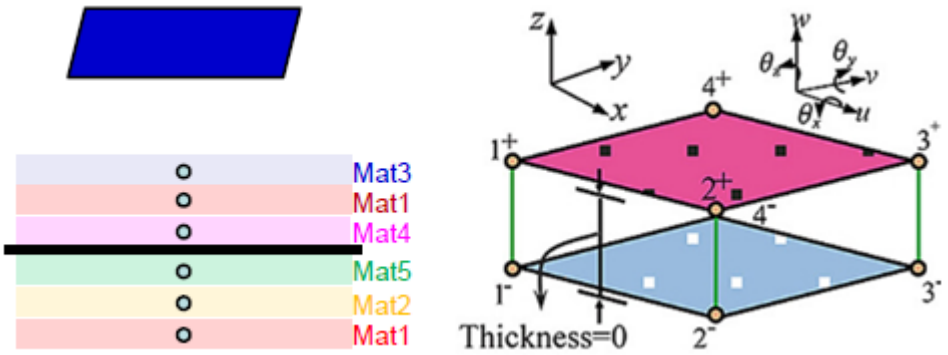

Figure 5.7 a) One shell layer composite b)Zero thickness cohesive element

Comparing the test results and our finite element model, we realize that the criteria affecting separation are mesh size, velocity and shell thickness. It is seen that these factors accelerate the onset of delamination time. Based on these factors, we created suitable DCB. Below it is available in detail about dimensions, velocity and material properties.

5.3 FE Modeling of Double Cantilever Beam

The dimensions of our DCB model, in which we used the same geometry in the test results, are 20 mm × 6.9 mm × 150 mm. Each of the upper and lower beams are consist of 5 laminates.

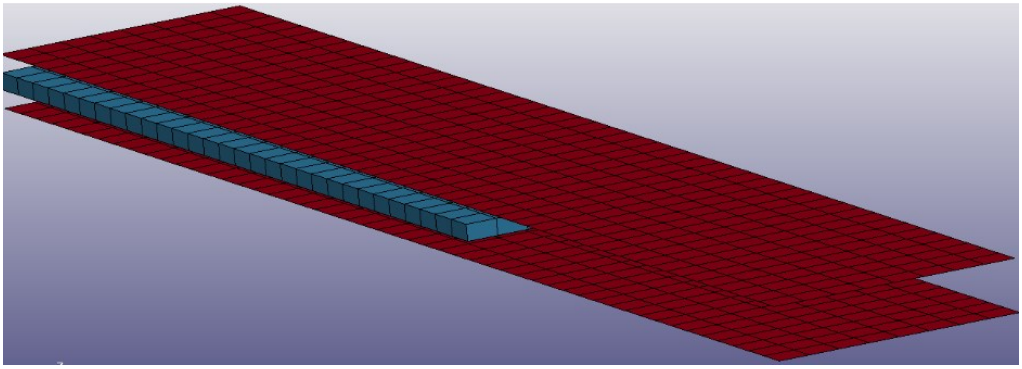

Figure 5.8 FE Modeling of Double Cantilever Beam

The preferred composite material for the lower and upper beams is pure polypropylene and is formed from shell form. Solid beam needs longer time to solve and complex due to more degree of freedom so we created shell DCB for linearly stress variation from front end to fixed end of beam and contributed fast solution time.

The aim of our shell DCB model is to reach the data closest to the experimental result. Therefore, we focus primarily on material properties in the cohesive zone like MAT 138 cohesive mixed mode data such as traction separation value, penalty stiffness, energy release rate, density and initial and final displacement values. Then, we focus on mesh size and dimension of DCB, velocity curve besides the density of the cohesive region. Based on this, the properties of the materials we use in numerical modeling are indicated in the table below and the active factors are adapted according to our composite and cohesive materials.

MAT 138 Cohesive Mixed Mode Card:

RO (density)	$9.550e-10\ [^{tonne}/_{mm^3}]$	T (peak traction in normal direction)	32 MPa
EN (penalty stiffness)	$2000\frac{N}{mm}^3$	S (peak traction in tangential direction)	16 MPa
ET (penalty stiffness)	$2000\frac{N}{mm}^3$	UND (δ_{fI})	0.0312 mm
GIC &GIIC (energy release rate)	0.5 N/mm	UTD (δ_{fII})	0.0625 mm

Table 5.2 Properties of cohesive material is used in FEM

As a result of our preference for explicit analysis, we find that the velocity curve is important in our model. Because the increase of the speed will decrease the rate of energy release rate, which will increase and stabilize by increasing the density of the cohesive material. So, we can say that velocity and density are inversely related. In our experiment, the total head opening displacement is 75 mm. But when we adapted this to the modeling, we had to assume the velocity curve as 80 mm/s. That means too much speed. For this reason, we gave the speed as 40 mm/s and aimed to establish the balance of the material card more easily. If we look at the density and mesh size of our composite material, it will be seen that it is not correct to enlarge the time interval to prevent splashing. That is why we cannot choose small speed and large time interval and prefer 40 mm/s.

The point to be kept in mind regarding the density of the cohesive material is that the delamination spread will increase as the density decreases. In order to establish this balance, we created the density value in Table 5.2.

The third factor is that increased traction value results in greater toughness. This gives us 2 important factors. Either we will increase the penalty stiffness and reduce the initial delamination and get a higher energy release rate or we will reduce the traction force, reduce the penalty stiffness and increase the initial delamination and see the corresponding increase in final delamination decrease energy release rate. All these optimisations are based studies of Bazant & Planas (1998) and Turon et al.(2007) as detailed in Figure 5.3.

By balancing the three factors we explained above, we were able to reach a very close conclusion with our experiment. But a fourth factor, mesh size, is our key point and the only determining factor in our load-displacement curve. Because there are 2 factors that can bring this curve to the same conclusion as our experiment: height and mesh size. Since we used 6.9 mm height in our experiment and we could not change it this fixed value, we focused on the mesh size. Minor changes in some values of the composite material whose properties are given below did not affect the result of the load-displacement curve. Therefore, we obtained a result closer to our experiment by changing the mesh size.

MAT 54 Enhanced Composite Damage Material Card:

Density	$7.5e-10\ [^{tonne}/_{mm^3}]$	EA (Young modulus in longitudinal direction)	$5500[\frac{N}{mm^2}]$
Model mesh size	4 mm	EB (Young modulus in transverse direction)	$5699\ [\frac{N}{mm^2}]$
Dimensions of beam	$20 \times 150 \times 6.9\ mm$	GAB (Shear modulus ab)	800 MPa
Layers' number of beam (2h)	10 layers	GBC (Shear modulus bc)	800 MPa

Tablo 5.3 Properties of composite material in DCB model

In the next title, the effect of mesh size and other factors is more effectively explained in comparisons of experimental and analysis results.

5.4 Comparison Between Experimental Results and FEM Results

We first did our model with mesh size of 2.5 mm and then 2 mm. However, since the load-displacement curve plot was lower than the experimental results, we used 4 mm mesh size. The coarse mesh size gave a closer result to our test result, even though it made more fluctuations in the graph in our model, in which we chose the 2*2 Gaussian integration.

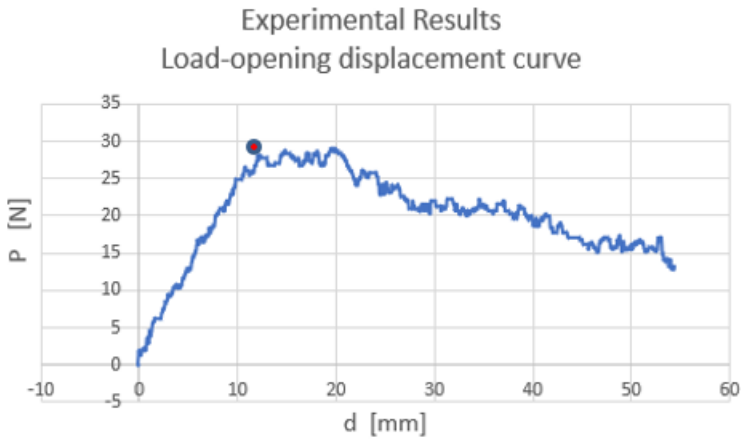

Figure 5.9: Load-opening displacement of DCB experiment result

It is seen that a maximum load of 30 N was applied in both load-displacement curves and this was at 11 mm total head opening displacement. The reason why this displacement is 25 mm in numerical modeling is because our speed is 40 mm/s. Considering the suitability of other parameters in the velocity curve where time intervals need to be arranged, it is seen that the closest result is by choosing this curve. Although the speed of 80 mm/s was thought to give the same result as in our experiment, the excessive reduction of the energy release rate made our optimization difficult.

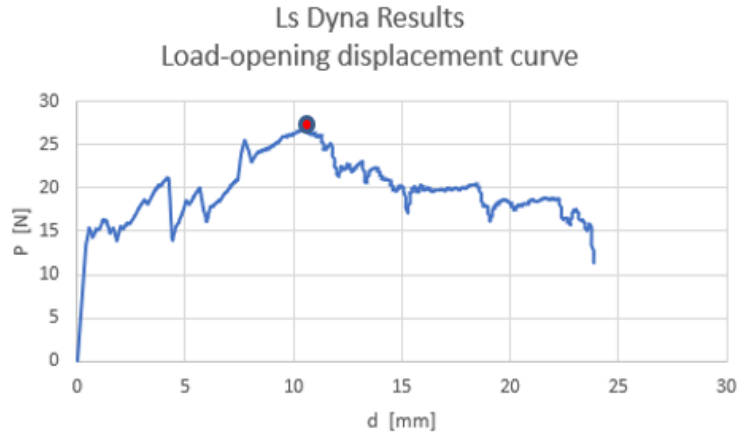

Figure 5.10: Load-opening displacement of DCB FEM result

The energy release rate value, in which the adhesive material plays an effective role on the speed and penalty stiffness of our model, is 0.5 $^{N}/_{mm}$, and this rate coincides with our test and test results

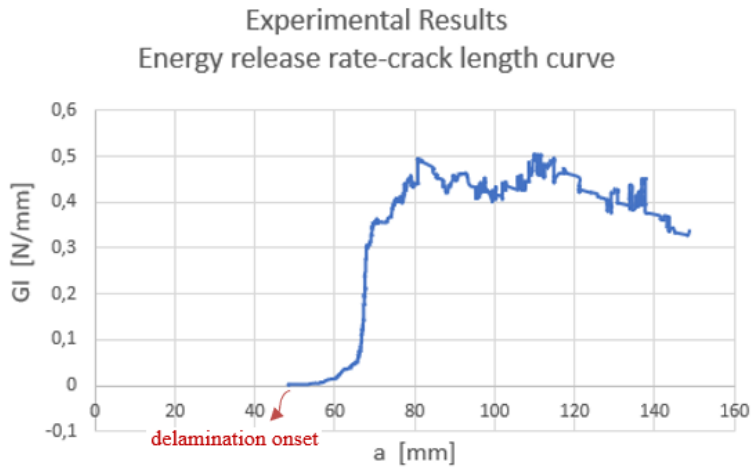

Figure 5.11 Energy release rate-crack length curve of DCB experiment

The energy release rate value, in which the adhesive material plays an effective role on the speed and penalty hardness of our model, is 0.5 N/mm3, and this rate coincides with our test and test results.

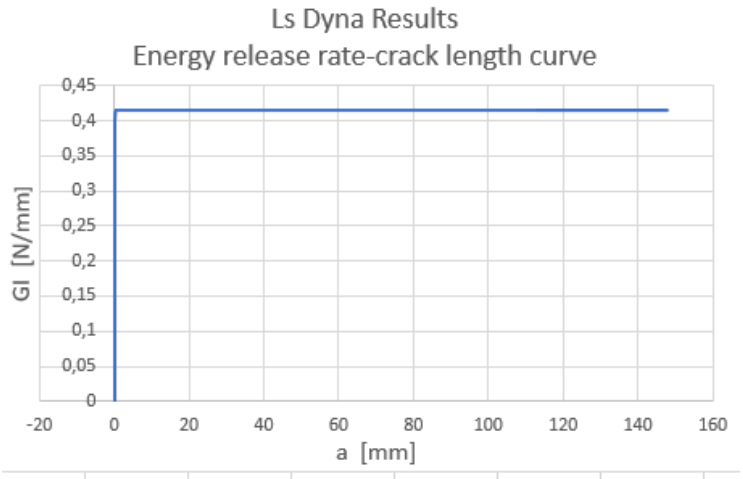

Figure 5.12 Energy release rate-crack length curve of DCB experiment

It is seen that DCB, which we modeled with test and ls dyna, gives similar results.

Conclusion

It can be said that our DCB model provides more precision and less cost in a short time by using the shell form rather than the solid form. We can say that the necessary and optimization can be successfully achieved with Ls-dyna to achieve the equivalent results of our DCB model, which we ensured its integrity with hot compaction in our experiment, and that it can be achieved with the energy release rate, speed, penalty stiffness and the peak traction to achieve this.

We say that the similarity of the analysis results with the test results in the load-displacement curve of our DCB model, which is the reference by keeping the height constant, is possible by changing only mesh size.

Computational time could be reduced by loading rate scaling and mass scaling in explicit analyse and it is limited in time step by the element size and the speed sound.Another advantage of explicit analysis is the less numerical effort required to internal forces. When we look at the results of the models, we see that the coarser mesh size completes the analysis in a short time and the geometry of model has a positive contribution on delamination length.

REFERENCES

[1] L.-D. A. W. Group, "2011 LS-DYNA Aerospace Working Group Modeling Guidelines Document V11-1," 2019.

[2] K. Song, C. Davila, and C. Rose, "Guidelines and parameter selection for the simulation of progressive delamination," *2008 ABAQUS User's Conf.*, pp. 1–15, 2008, [Online]. Available: http://www.simulia.com/forms/world/pdf2008/SONG-AUC2008.pdf.

[3] A. R. Khoei, H. Moslemi, and M. Sharifi, "Three-dimensional cohesive fracture modeling of non-planar crack growth using adaptive FE technique," *Int. J. Solids Struct.*, vol. 49, no. 17, pp. 2334–2348, 2012, doi: 10.1016/j.ijsolstr.2012.04.036.

[4] P. Ladeveze and E. LeDantec, "Damage modelling of the elementary ply for laminated composites," *Compos. Sci. Technol.*, vol. 43, no. 3, pp. 257–267, 1992, doi: 10.1016/0266-3538(92)90097-M.

[5] G. R. Irwin and D. C. Washington, "G. R. Irwin, 'Analysis of stresses and strains near the end of a crack traversing a plate'. J. Applied Mechanics, 24,(1957) 361–364." pp. 361–364, 1957.

[6] H. Ben Kahla, "MASTER ' S THESIS Models for bending stiffness in laminates with intralaminar and interlaminar damage," 2014.

[7] Y. Ousset, "Numerical simulation of delamination growth in layered composite plates," *Eur. J. Mech. A/Solids*, vol. 18, no. 2, pp. 291–312, 1999, doi: 10.1016/S0997-7538(99)80017-5.

[8] A. Turon, P. P. Camanho, J. Costa, and C. G. Dávila, "An Interface Damage Model for the Simulation of Delamination Under Variable-Mode Ratio in Composite Materials," *Nasa/Tm-2004-213277*, no. NASA/TM-2004-213277, 2004, [Online]. Available: http://hdl.handle.net/2060/20040171493.

[9] C. G. Dávila, P. P. Camanho, and A. Turon, "Cohesive elements for shells," *Nasa/Tp-2007-214869, L-19341*, no. April 2007, p. 27, 2007.

[10] H. C. Cohen *et al.*, *Response of resistant ventricular tachycardia to bretylium. Relation*

to site of ectopic focus and location of myocardial disease., vol. 47, no. 2. 1973.

[11] X. P. Xu and A. Needleman, "Numerical simulations of fast crack growth in brittle solids," *J. Mech. Phys. Solids*, vol. 42, no. 9, pp. 1397–1434, 1994, doi: 10.1016/0022-5096(94)90003-5.

[12] P. G. Bergan and E. Mollestad, "An automatic time-stepping algorithm for dynamic problems," *Comput. Methods Appl. Mech. Eng.*, vol. 49, no. 3, pp. 299–318, 1985, doi: 10.1016/0045-7825(85)90127-6.

[13] M. May and S. R. Hallett, "Under Fatigue Loading Using Interface Elements," *Composites*, no. 1, pp. 1–2.

[14] I. Scheider and W. Brocks, "Simulation of cup - cone fracture using the cohesive model," *Eng. Fract. Mech.*, vol. 70, no. 14, pp. 1943–1961, 2003, doi: 10.1016/S0013-7944(03)00133-4.

[15] J. W. Hutchinson and V. Tvergaard, "The relation between crack growth resistance and fracture process parameters elastic-plastic solids," *J. Mech. Phys. Solids*, vol. 40, no. 6, pp. 1377–1397, 1992.

[16] X. Chao, L. Qi, W. Tian, K. Yang, and H. Li, "Evaluation for interfacial fracture of fiber-reinforced pyrocarbon matrix composites by using a zero-thickness cohesive approach," *J. Alloys Compd.*, vol. 820, p. 153378, 2020, doi: 10.1016/j.jallcom.2019.153378.

[17] G. T. Camacho and M. Ortiz, "Computational modelling of impact damage in brittle materials," *Int. J. Solids Struct.*, vol. 33, no. 20–22, pp. 2899–2938, 1996, doi: 10.1016/0020-7683(95)00255-3.

[18] M. Bari, "A finite element study of shell and solid element performance in crash- box simulations," 2015.

[19] G. N. Barenblatt, "Arlington Hall Station," *Zhurnal Prikl. Mekhaniki i Tec.*, 1962.

[20] A. Needleman, "A continuum model for void nucleation by inclusion debonding," *J. Appl. Mech. Trans. ASME*, vol. 54, no. 3, pp. 525–531, 1987, doi: 10.1115/1.3173064.

[21] A. Needleman, "Some issues in cohesive surface modeling," *Procedia IUTAM*, vol. 10, pp. 221–246, 2014, doi: 10.1016/j.piutam.2014.01.020.

[22] P. P. Camanho, C. G. Dávila, and M. F. S. F. De Moura, “Mixed-mode Progressive Delamination in Composite Materials,” *J. Compos. Mater.*, vol. 37, no. May 2014, pp. 1415–1438, 2003, doi: 10.1177/002199803034505.

[23] A. Hillerborg, M. Modéer, and P. E. Petersson, “Analysis of crack formation and crack growth in concrete by means of fracture mechanics and finite elements,” *Cem. Concr. Res.*, vol. 6, no. 6, pp. 773–781, 1976, doi: 10.1016/0008-8846(76)90007-7.

[24] M. L. Falk, A. Needleman, and J. R. Rice, “A critical evaluation of dynamic fracture simulations using cohesive surfaces,” 2001, [Online]. Available: http://arxiv.org/abs/cond-mat/0106304.

[25] Y. Mi, M. A. Crisfield, G. A. O. Davies, and H. B. Hellweg, “Progressive delamination using interface elements,” *J. Compos. Mater.*, vol. 32, no. 14, pp. 1246–1272, 1998, doi: 10.1177/002199839803201401.

[26] P. W. Harper and S. R. Hallett, “Cohesive zone length in numerical simulations of composite delamination,” *Eng. Fract. Mech.*, vol. 75, no. 16, pp. 4774–4792, 2008, doi: 10.1016/j.engfracmech.2008.06.004.

[27] M. Meo and E. Thieulot, “Delamination modelling in a double cantilever beam,” *Compos. Struct.*, vol. 71, no. 3–4, pp. 429–434, 2005, doi: 10.1016/j.compstruct.2005.09.026.

[28] P. P. Camanho and C. G. Davila, “Mixed-Mode Decohesion Finite Elements for the Simulation of Delamination in Composite Materials,” *NASA Tech. Pap.*, vol. 211737, no. June, p. 42, 2002, [Online]. Available: http://citeseerx.ist.psu.edu/viewdoc/download?doi=10.1.1.8.267&rep=rep1&type=pdf.

[29] A. Turon, C. G. Dávila, P. P. Camanho, and J. Costa, “An engineering solution for mesh size effects in the simulation of delamination using cohesive zone models,” *Eng. Fract. Mech.*, vol. 74, no. 10, pp. 1665–1682, 2007, doi: 10.1016/j.engfracmech.2006.08.025.

[30] G. Alfano and M. A. Crisfield, “Finite element interface models for the delamination analysis of laminated composites: Mechanical and computational issues,” *Int. J. Numer. Methods Eng.*, vol. 50, no. 7, pp. 1701–1736, 2001, doi: 10.1002/nme.93.

[31] M. S. S. Prasad, C. S. Venkatesha, and T. Jayaraju, “Experimental Methods of

Determining Fracture Toughness of Fiber Reinforced Polymer Composites under Various Loading Conditions," *J. Miner. Mater. Charact. Eng.*, vol. 10, no. 13, pp. 1263–1275, 2011, doi: 10.4236/jmmce.2011.1013099.

[32] A. B. de Morais and A. B. Pereira, "Mixed mode I + II interlaminar fracture of glass/epoxy multidirectional laminates - Part 1: Analysis," *Compos. Sci. Technol.*, vol. 66, no. 13, pp. 1889–1895, 2006, doi: 10.1016/j.compscitech.2006.04.006.

[33] Z. P. Bažant and Q. Yu, "Size Effect in Fracture of Concrete Specimens and Structures: New Problems and Progress," *Acta Polytech.*, vol. 44, no. 5–6, pp. 7–15, 2004, doi: 10.14311/608.

[34] A. C. Society, "NOTICE : This standard has either been superseded and replaced by a new version or discontinued . Contact ASTM International (www.astm.org) for the latest information . Standard Test Method for Measurements of Aqueous Solubility 1," vol. 11, no. Reapproved, pp. 1–3, 1993.

[35] S. Cicero, J. a Alvarez, and R. Lacalle, "B . INTRODUCTION TO ASSESSMENT PROCEDURES FOR CRACKED Critical conditions Critical conditions," *Education*, pp. 40–62, 2001.

[36] M. Saeedi, M. Azadi, M. Mokhtarishirazabad, and P. Lopez-Crespo, "Numerical simulations of carbon/epoxy laminated composites under various loading rates, comparing extended finite element method and cohesive zone modeling," *Mater. Des. Process. Commun.*, no. June, pp. 1–20, 2020, doi: 10.1002/mdp2.198.

[37] F. Daricik, "Mesh size sensitivity analysis for interlaminar fracture of the fiber-reinforced laminated composites," *J. Eng. Fiber. Fabr.*, vol. 14, 2019, doi: 10.1177/1558925019883460.

[38] J. J. C. Pituba and E. A. S. Neto, "Modeling of unilateral effect in brittle materials by a mesoscopic scale approach," *Comput. Concr.*, vol. 15, no. 5, pp. 735–758, 2015, doi: 10.12989/cac.2015.15.5.735.

[39] The Arup Campus, "Introduction to Composites Modelling in LS-DYNA," vol. 44, no. June, pp. 0–70, 2018.

[40] P. Chatla, "Ls-Dyna For Crashworthiness of Composite Structures," *Aerosp. Eng.*, vol. Master, p. 101, 2012.

[41] B. Gözlüklü, “Delamination Analysis by Using Cohesive Interface Elements in Laminated Composite,” *Master Thesis*, no. August, p. 149, 2009.

[42] M. Thesis, F. H. Hermes, P. A. Technologies, and P. M. Group, “Process zone and cohesive element size in numerical simulations of delamination in bi-layers,” 2010.

[43] S. Solaimurugan and R. Velmurugan, “SCIENCE AND Influence of in-plane fibre orientation on mode I interlaminar fracture toughness of stitched glass / polyester composites,” vol. 68, pp. 1742–1752, 2008, doi: 10.1016/j.compscitech.2008.02.008.